

Remote spectral detection of biodiversity effects on forest biomass

Laura J. Williams ^{1,2} , Jeannine Cavender-Bares ¹ , Philip A. Townsend ^{1,2} , John J. Couture ^{1,5} , Zhihui Wang ^{1,2} , Artur Stefanski ^{1,2} , Christian Messier ^{6,7} and Peter B. Reich ^{1,2} ,

Quantifying how biodiversity affects ecosystem functions through time over large spatial extents is needed for meeting global biodiversity goals yet is infeasible with field-based approaches alone. Imaging spectroscopy is a tool with potential to help address this challenge. Here, we demonstrate a spectral approach to assess biodiversity effects in young forests that provides insight into its underlying drivers. Using airborne imaging of a tree-diversity experiment, spectral differences among stands enabled us to quantify net biodiversity effects on stem biomass and canopy nitrogen. By subsequently partitioning these effects, we reveal how distinct processes contribute to diversity-induced differences in stand-level spectra, chemistry and biomass. Across stands, biomass overyielding was best explained by species with greater leaf nitrogen dominating upper canopies in mixtures, rather than intraspecific shifts in canopy structure or chemistry. Remote imaging spectroscopy may help to detect the form and drivers of biodiversity-ecosystem function relationships across space and time, advancing the capacity to monitor and manage Earth's ecosystems.

Biodiversity is changing at local to global scales in response to habitat degradation and fragmentation, climate change, nutrient enrichment, species introductions and more¹⁻⁴. Meanwhile, ecosystem functions and the ecosystem services that support life depend on biodiversity^{2,5,6}. Yet, how relationships between biodiversity and ecosystem function vary across space and time remains poorly understood². Local-scale experiments dominate understanding of biodiversity–ecosystem function relationships⁷. Theory^{2,3,8,9} and recent empirical studies indicate that the positive relationships predominant at local scales¹⁰ ought to persist or strengthen across larger scales of space and time^{11–13}.

There are at least two kinds of scaling relevant to this issue. First, it is unknown whether biodiversity–ecosystem function relationships at fine scales differ systematically from those at larger spatial grains (for example, 1 m², 100 m², 1 km² and 100 km²), that is, areal scale dependency. This dependency merits evaluation because relationships may change, even in direction, with spatial grain 14. Second, it remains unclear whether relationships found in experiments and observations within limited contexts apply regardless of contexts and community types; in other words, whether relationships at the fine-scale neighbourhoods where most biodiversity–ecosystem function mechanisms occur can be extrapolated to other similar domains in different systems.

The data needed to assess either kind of scaling of biodiversity-ecosystem function relationships are challenging to collect with traditional field-based methods but may be complemented with airborne or satellite imaging spectroscopy^{15–17}. Given increasing risks of biodiversity loss and climate change^{2,6,18}, the development of effective approaches to remotely sense diversity effects on ecosystem functions and properties that can advance theory, understanding and quantification of how relationships scale across space

and time is being called for ^{15,19,20}. If achieved, these advances will inform management options for Earth's ecosystems to help simultaneously meet global biodiversity, sustainability and climate change goals ^{6,18,21}. Here, we present and test an approach for remotely detecting and partitioning biodiversity effects ²² on forest biomass production, an important ecosystem function, by spectrally identifying the diversity and stem biomass of forest stands.

While imaging spectroscopy is becoming increasingly accessible²³, its potential is only beginning to be revealed. To date, ecological applications of imaging spectroscopy have included detecting biodiversity through identifying species or spectral signatures of diversity^{24–27}, measuring functionally important attributes of vegetation such as canopy chemistry^{28–30} or disease³¹, and estimating biomass, productivity and photosynthetic capacity^{32–34}. However, imaging spectroscopy has not yet been applied to characterize the effects of biodiversity on ecosystem function.

Beyond documenting the existence of biodiversity–ecosystem function relationships, we need better capacity to decipher the mechanisms that drive these relationships to predict the consequences of biodiversity change, especially in changing environments. In forests, diversity has been found to enhance productivity and biomass both in small-scale tree experiments and in studies of natural stands^{13,35,36}, and recent efforts have shifted toward understanding underlying mechanisms^{37–39}. Enhanced productivity in mixed-species stands may be a consequence of resource partitioning among species that leads to reduced competition, competitive imbalances that lead to the dominance of a highly productive species, facilitation that ameliorates light or microclimatic stress and/or trophic interactions that reduce losses to herbivory or disease^{40–43}. Alongside mechanisms reliant on differences among species, intraspecific variation may also shape diversity–productivity relationships³⁷.

¹Department of Ecology, Evolution and Behavior, University of Minnesota, St Paul, MN, USA. ²Department of Forest Resources, University of Minnesota, St Paul, MN, USA. ³Department of Forest and Wildlife Ecology, University of Wisconsin-Madison, Madison, WI, USA. ⁴Department of Entomology, Purdue University, West Lafayette, IN, USA. ⁵Department of Forestry and Natural Resources, Purdue University, West Lafayette, IN, USA. ⁶Centre for Forest Research, Université du Québec à Montréal, Montréal, Quebec, Canada. ⁷Institut des sciences de la forêt tempérée, Université du Québec en Outaouais, Ripon, Quebec, Canada. ⁸Hawkesbury Institute for the Environment, Western Sydney University, Penrith, New South Wales, Australia. [™]e-mail: will3972@umn.edu; cavender@umn.edu

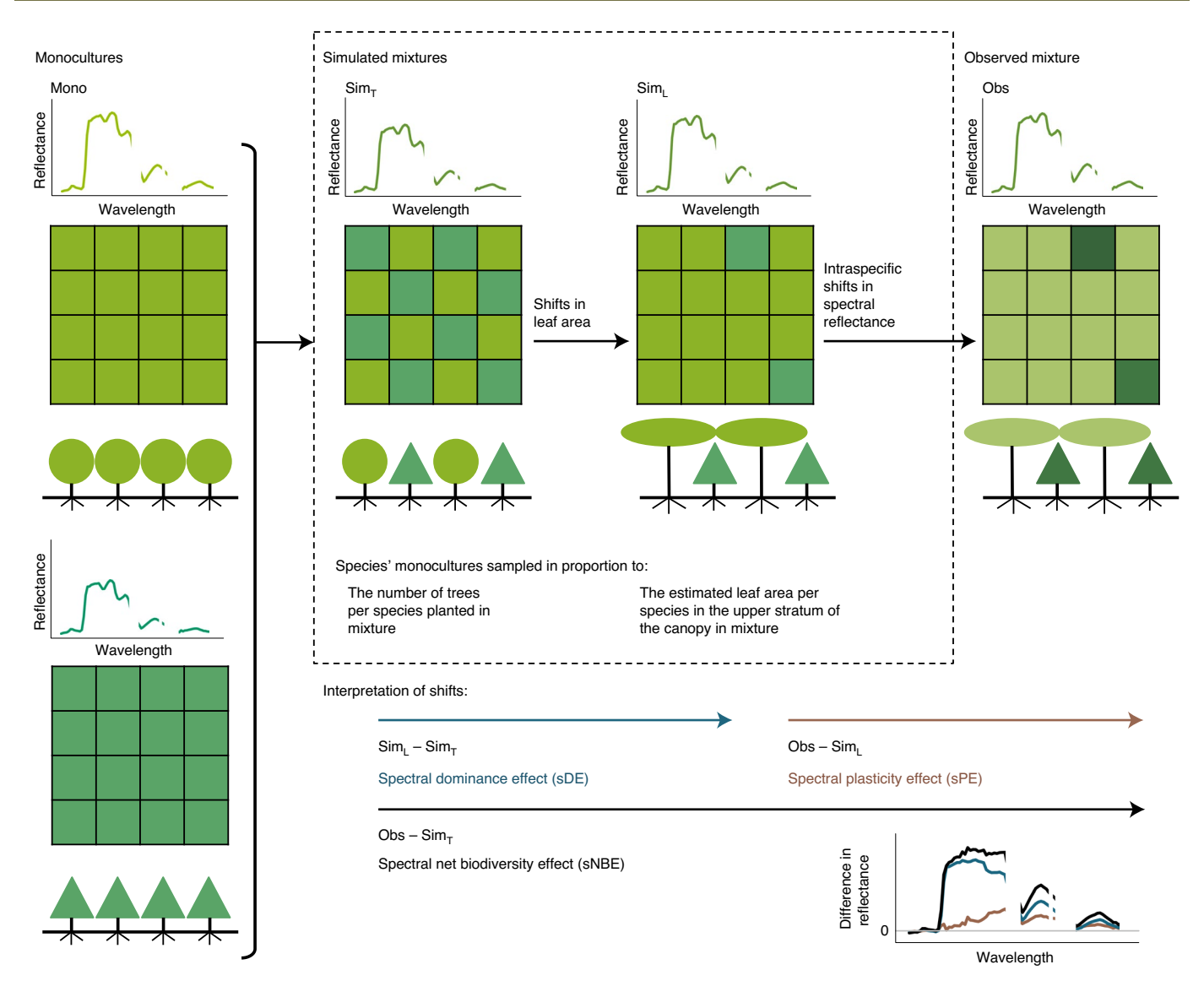


Fig. 1 | Simulations to assess spectral diversity effects. We simulated mixtures from monocultures in two ways—according to the number of trees (T) per species planted in mixture (Sim_T) and according to the upper canopy leaf area (L) per species in mixture (Sim_T)—to decipher the relative contributions of the sDE and sPE to the sNBE. In this hypothetical example, two species (circles and triangles) are depicted in monoculture, simulated mixtures and an observed mixture. Differences in colour between monocultures and mixture represent intraspecific differences in canopy traits. Each assemblage is illustrated in cross-section, from overhead (depicted in a grid to represent pixels) and as a mean reflectance spectrum. The differences in spectral reflectance captured by the sNBE, sDE and sPE are also shown.

We propose that differences in spectral reflectance between mixed-species stands and monocultures will contain signals of diversity effects on biomass and be separable into components related to the drivers of diversity-enhanced biomass (Fig. 1). The spectral reflectance of canopies is affected by leaf traits—their chemistry and morphology—and canopy structure, including the number, angle and spatial distribution of leaves within and among crowns. Differences in spectral reflectance between a mixed-species stand and the mean of monocultures of the same species may come from two main sources: (1) shifts in the relative dominance of different species in the uppermost stratum of the canopy and (2) plastic or intraspecific shifts in spectral reflectance resulting from species expressing different leaf or crown traits in mixture. Here, we propose an approach to partition the contributions of these mechanisms to the net biodiversity effect.

Differences in spectral reflectance between mixtures and monocultures may also be linked to well-understood chemical and

physiological determinants of forest productivity such as foliar nitrogen concentration. Canopy nitrogen is a key driver of forest productivity⁴⁴ because the nitrogen-containing compounds of RuBisCO and chlorophyll determine the biochemical fixation of carbon. Canopy nitrogen also drives variation in spectral reflectance and is measurable from spectroscopic data^{28,29}. We further suggest that increased stem biomass in mixed-species stands will correspond with spectrally detectable increases in canopy nitrogen, which may arise through the dominance of species with greater leaf nitrogen or through intraspecific increases in either leaf nitrogen or in the density of leaves within crowns.

In this study, we assess whether diversity effects on biomass, and their underlying ecological drivers, can be spectrally detected in tree communities; and whether these effects correspond with spectrally detectible shifts in canopy nitrogen. The capacity for imaging spectroscopy to detect relationships between biodiversity and biomass can be assessed rigorously in a controlled setting

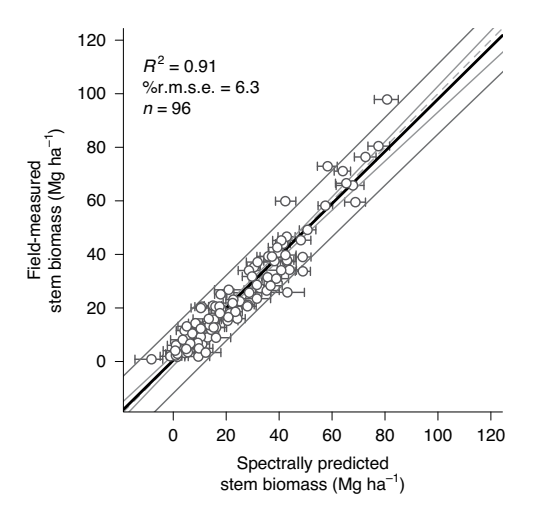


Fig. 2 | Prediction of stem biomass from spectra. Field-measured stem biomass and PLSR model predictions of stem biomass. The model was calibrated using data from the fifth and sixth growing seasons with predictions shown for the independent validation subset of stands which were selected in stratified random fashion from both growing seasons (Methods). Error bars show 95% confidence intervals among 1,000 model iterations. The thick line represents the regression line, dark grey lines represent the 95% prediction interval and light grey lines represent the 95% confidence interval of the models: the dashed grey line shows 1:1.

where one can easily manipulate species mixtures and accurately quantify effects on the ground. To this end, we combined airborne (AVIRIS-Next Generation (NG)) imaging spectroscopy data with field-collected data across a tree-diversity experiment in Minnesota, United States⁴⁵. The experiment was composed of 192 young stands of monocultures and different mixtures of two and six species (Methods). Data were collected for each of 2 years, when stands were in their fifth and sixth growing seasons and had largely developed closed canopies (mean leaf area index, LAI, of 4.5 and 5.9, respectively).

Results

Our approach of detecting biodiversity effects on biomass depends upon accurate spectral detection of biomass differences among stands. We predicted stem biomass using partial least squares regression (PLSR). The model was calibrated onsite with data from both growing seasons and leveraged full-range spectral reflectance (400–2,500 nm). We found that the PLSR model performed well, explaining 91% of variation among stands in stem biomass, with a relative root mean square error (%r.m.s.e.) of 6.3% for independent data (Fig. 2 and Extended Data Fig. 1). As a point of contrast, a common multispectral index, the normalized difference vegetation index (NDVI), explained only 21-27% of variation in stem biomass among stands (Supplementary Fig. 1). Important wavelengths within the PLSR model occurred throughout the spectrum, particularly at the red-edge of the visible and near-infrared (NIR) around 755 nm, the NIR (~935 nm), the NIR to short-wave infrared (SWIR) transition (~1,340 nm) and in the SWIR (~1,800 nm) (Extended Data Fig. 2). These wavelengths leverage features at the red-edge and in the NIR that are generally associated with canopy and foliar structure and biomass, and water absorption features (SWIR) that also correlate with total foliar biomass.

The net biodiversity effect (NBE) on stem biomass was calculated as the difference between the stem biomass of a species mixture and the average stem biomass of monocultures of the same set of species²² (Methods). We calculated the spectral net biodiversity effect (sNBE) in the same manner: as the difference between the spectral

reflectance of a mixed-species stand and the reflectance averaged (via a simulation procedure) across monocultures of the same species (Fig. 1). Spectral reflectance observed in mixed-species stands (Obs) differed from the spectral reflectance simulated (Sim) for mixed-species stands from monocultures of the same species based on the proportion of trees planted (T) (Sim_T). These differences in spectral reflectance between species mixtures and monocultures predicted diversity effects on stem biomass. Applying the PLSR model for stem biomass to the stand-level observed spectra (Obs) and simulated spectra (Sim_T) and then calculating the difference in predicted stem biomass—that is, the sNBE on stem biomass explained 54-69% of variation among stands in field-measured diversity-enhanced stem biomass (NBE) each year (Fig. 3a,d). These results indicate that the upper canopy layers captured by remote spectroscopic imaging are informative in assessing diversity effects on stem biomass, at least within our young stands. Stands that had a positive NBE on stem biomass (that is, overyielded) tended to have higher reflectance in the NIR and lower in SWIR (especially 1,500-1,750 nm), which relate to higher foliar biomass and canopy water content, than in their monoculture simulations (Extended Data Fig. 3).

To assess the relative importance of species' dominance of the upper canopy and intraspecific variation to diversity-induced shifts in spectral reflectance and stem biomass, we separated sNBE into two additive components—a spectral dominance effect (sDE) and a spectral plasticity effect (sPE) (Fig. 1). Diversity-enhanced stem biomass on average across our stands was most attributable to shifts in species' dominance of the upper canopy as opposed to plastic shifts in leaf traits or canopy structure. Across all stands, the sDE on stem biomass explained 43-44% of variation in the field-measured NBE on stem biomass (Fig. 3b,e) and 52-64% of the spectrally measured NBE on stem biomass (Extended Data Fig. 4). The sPE on stem biomass explained little variation in the NBE on stem biomass across all stands, explaining only 0-3% of variation in the field-measured NBE on stem biomass and 3-11% of the spectrally measured NBE on stem biomass (Fig. 3c,f and Extended Data Fig. 4). However, the relative contribution of the spectral dominance and sPEs to sNBE on stem biomass differed among stands (Extended Data Fig. 4). Diversity effects within stands were largely consistent in direction and relative magnitude between our study years (Extended Data Fig. 4), indicating stability in the drivers of diversity-enhanced stem biomass on a given stand during these early stages of stand development.

We mapped canopy nitrogen with spectra (Methods; Extended Data Fig. 5) to assess whether differences in canopy nitrogen between mixed-species stands and monocultures corresponded with diversity-enhanced stem biomass. Spectrally predicted canopy nitrogen was closely associated with canopy nitrogen based on field measurements and explained 33-37% of variation among stands in stem biomass in each year (Extended Data Fig. 6). The NBE on spectrally predicted canopy nitrogen was also positively associated with the field-measured NBE on stem biomass, explaining nearly one-third (29-32%) of variation among stands each year (Fig. 4a,d). Moreover, by applying our spectral partitioning approach (Fig. 1) to spectrally predicted canopy nitrogen, we assessed whether diversity-driven differences in canopy nitrogen were attributable to shifts in the upper canopy dominance of species with different canopy nitrogen concentration or plastic shifts in species' canopy nitrogen concentration. Across stands, the field-measured NBE on stem biomass was more closely associated with the sDE on canopy nitrogen ($R^2 \ge 0.33$) than the sPE on canopy nitrogen ($R^2 \le 0.09$; Fig. 4b,c,e,f).

The steps above, that outline our approach to assessing diversity effects on stem biomass, require field-based knowledge of the species composition of stands—knowing which stands are monocultures and knowing species' relative abundances within

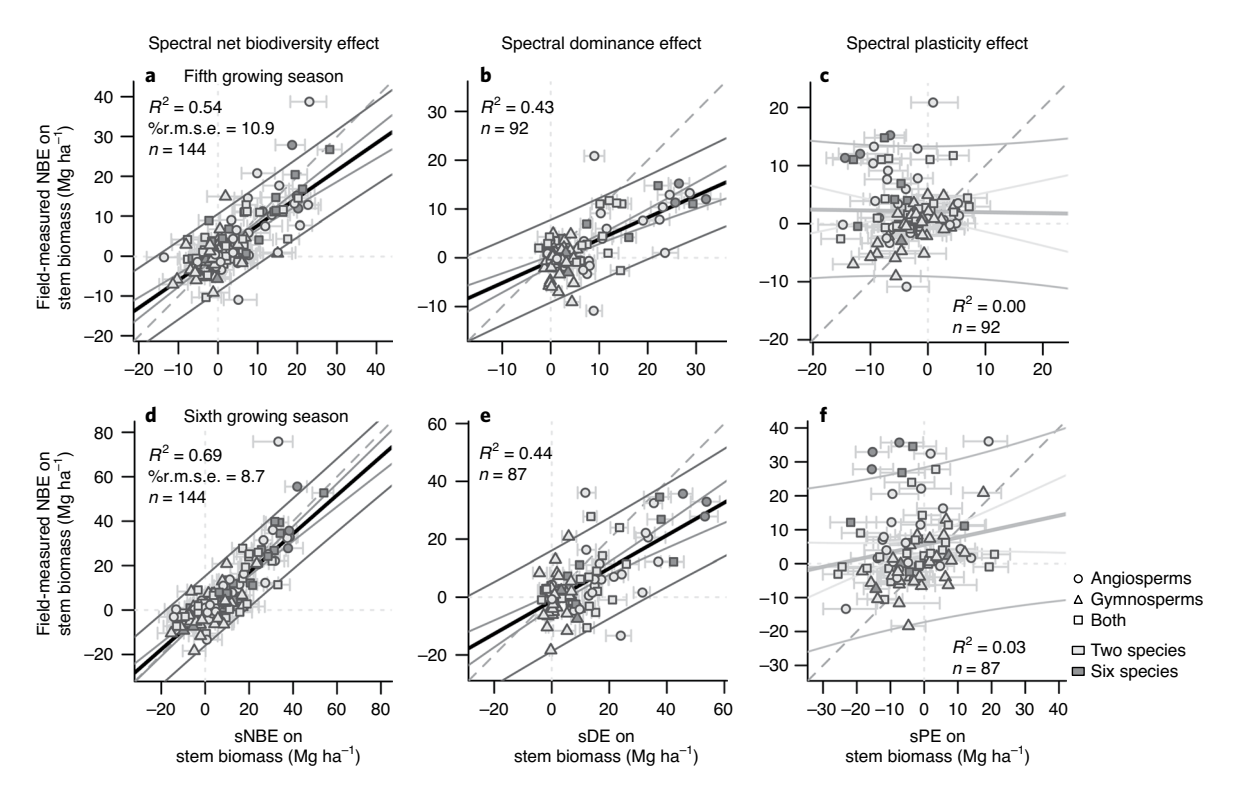


Fig. 3 | Spectral diversity effects on stem biomass and the field-measured NBE. a-f, NBE on stem biomass and the sNBE (\mathbf{a},\mathbf{d}) , sDE (\mathbf{b},\mathbf{e}) and sPE (\mathbf{c},\mathbf{f}) in the fifth $(\mathbf{a}-\mathbf{c})$ and sixth $(\mathbf{d}-\mathbf{f})$ growing seasons. Error bars show 95% confidence intervals among model iterations. The thick line represents the regression line (significant for sNBE and sDE, P < 0.001; but not for sPE, P = 0.807, 0.086 in the fifth and sixth growing seasons, respectively). Dark grey lines represent the 95% prediction interval and light grey lines the 95% confidence interval of the models; the dashed grey line shows 1:1.

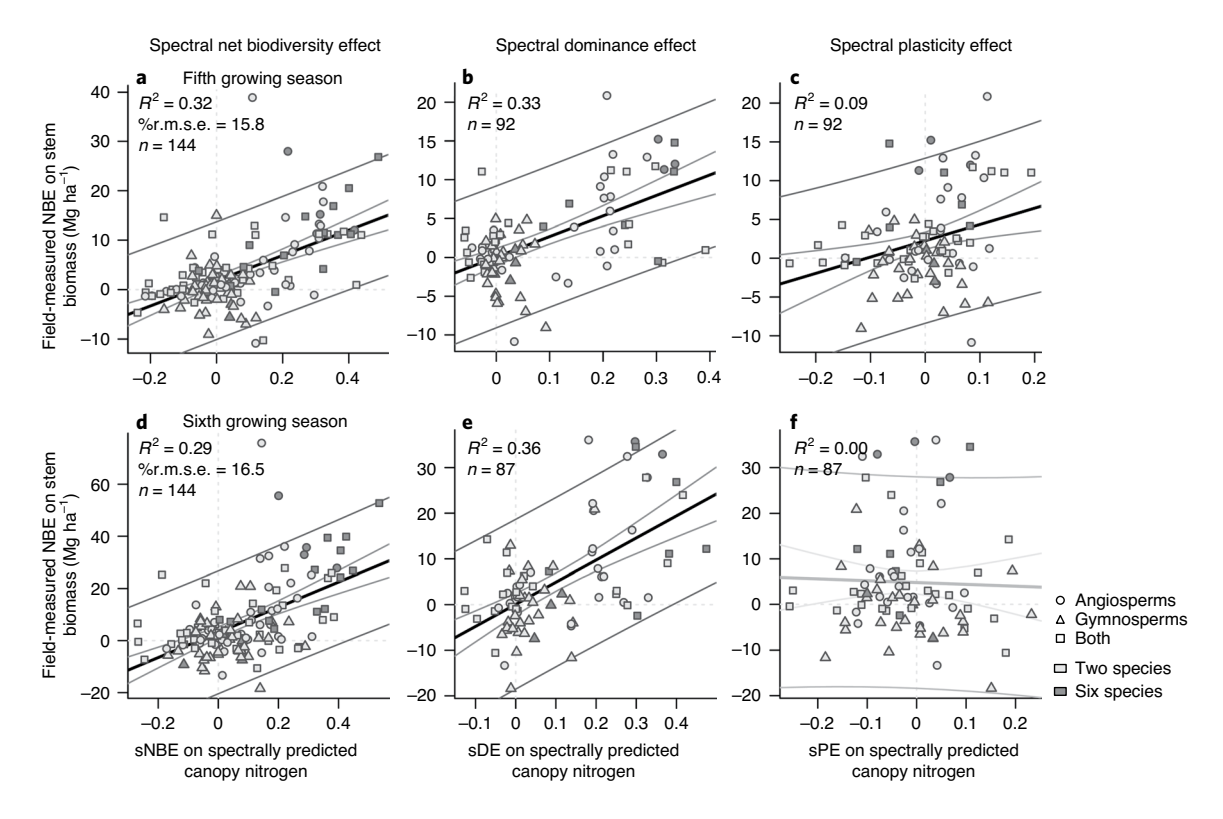


Fig. 4 | Diversity effects on spectrally predicted canopy nitrogen and the field-measured NBE on stem biomass. a-f, NBE on stem biomass and the sNBE (**a,d**), the sDE (**b,e**) and the sPE (**c,f**) on spectrally predicted canopy nitrogen (%) in the fifth (**a-c**) and sixth growing seasons (**d-f**). The thick line represents the regression line (significant for all panels, $P \le 0.003$; except **f**, P = 0.761), the dark grey lines represent the 95% prediction interval and light grey lines represent the 95% confidence interval of the models.

mixed-species stands. Although necessary as a proof of concept that spectra can detect biodiversity effects, this approach cannot be used in naturally assembled forests where the species composition of stands is unknown.

Thus, we also assessed whether spectra can identify the species composition of stands as well as diversity effects; that is, whether diversity effects on stem biomass may be entirely remotely detected. To do so, we began with a known species pool, trained models to discriminate among these species according to their spectral reflectance in monocultures (Methods; Extended Data Fig. 7) and applied these models to spectrally identify monoculture stands and the species composition of mixed-species stands (Methods; Extended Data Fig. 8).

We found that species could be distinguished in monoculture with high levels of accuracy (Extended Data Fig. 9). Applying these models across all stands sometimes inaccurately identified species' presence within stands—probably due to pixels containing mixtures of species, variable trait expression and thus reflectance of species in mixture, or missed detection of overtopped species (Extended Data Fig. 8). Using these spectrally identified monocultures and compositions of mixed-species stands, we repeated our approach of simulating the spectra of mixed-species stands (Fig. 1) and applying PLSR models to calculate the sNBE, sDE and sPE on stem biomass (Methods). By spectrally detecting both species composition and stem biomass, diversity effects on stem biomass could be predicted from remotely sensed imagery without explicit ground-based knowledge of species composition or relative abundance. The NBE on stem biomass predicted using only spectra (that is, when the species composition of stands was spectrally identified, sID; sNBE_{siD}) was significantly associated with the field-measured NBE on stem biomass ($R^2 = 0.27$, $t_{130} = 6.85$, P < 0.001 in the fifth growing season; $R^2 = 0.42$, $t_{130} = 9.73$, P < 0.001 in the sixth growing season). Moreover, the spectral dominance and plasticity effects on stem biomass predicted using only spectra (when composition was also spectrally predicted; sDE_{sID} and sPE_{sID}) explained 41-60% of variation among stands in the spectral dominance and sPEs on stem biomass calculated where stand composition was known (sDE and sPE) (Extended Data Fig. 10).

Discussion

By comparing spectrally assessed stem biomass in monocultures and mixed-species stands of young trees, we show how airborne imaging spectroscopy can be leveraged to detect patterns of diversity-enhanced biomass in forests (Fig. 1) and lend insight into the ecological processes that underlie these patterns (Figs. 3 and 4). While previous studies have shown how spectral measures of diversity may correspond with patterns of biomass⁴⁶, the extent to which imaging spectroscopy can identify diversity effects on biomass and underlying mechanisms, has not been demonstrated before.

Spectral signals of diversity-enhanced stem biomass were driven by differences between monocultures and mixtures in species' canopy dominance and/or intraspecific shifts in canopy structure or leaf traits. By separating diversity effects on spectrally detected stem biomass into effects attributable to spectral dominance and spectral plasticity, we found that shifts in species' dominance of the upper canopy best explained diversity-enhanced stem biomass on average across our stands (Fig. 3). This might well be different in other ecosystems and across time⁴⁷. Moreover, the relative contribution of different drivers of diversity effects depended on the species composition of stands (Extended Data Fig. 4). For instance, the sDE was prevalent in mixtures with angiosperms, consistent with these species possessing traits at the 'fast' end of the resource economics spectrum⁴⁸. The strong contribution of the sPE in mixtures of gymnosperms signals intraspecific shifts in their canopies consistent with community-driven shifts in species' crown and leaf traits^{39,49}. Trees were planted at the same density in all stands, thus the sDE implies that a species occupies a greater portion of the upper canopy per tree in mixture than it does in monoculture. Associated changes in canopy structure, such as a species having lower LAI than in monoculture, may manifest as a negative sPE; this was observed most prominently in mixtures containing angiosperms where the sPE often tempered strong sDEs.

One challenge in using optical remote sensing in forests is that the reflectance signal may saturate with increasing leaf layers and information about lower strata may be missed⁵⁰. Despite our young stands having LAI values comparable to mature forests44 (4.5 and 5.9 in the fifth and sixth growing seasons, respectively), biomass and diversity effects on stem biomass were strongly evident in spectra. Tree growth is typically light-limited within closed canopy forests^{51,52}. The upper canopy layers that remotely sensed imaging spectroscopy detects are the same layers that intercept most light and, in so doing, tend to dominate forest productivity⁵³. Our approach of detecting diversity-enhanced biomass might be less effective when stands have stratified canopies with subdominant species that contribute considerable biomass because spectra might miss the biomass contributions of overtopped trees. In such instances, detecting diversity-enhanced production may be more effective as overtopped trees contribute less to annual production.

Productivity (measured as stem biomass growth) was closely associated with standing stem biomass on our young stands $(R^2 = 0.94 - 0.97;$ Supplementary Fig. 2) and analyses that predicted and partitioned diversity effects on productivity rather than biomass led to comparable findings (Supplementary Table 1 and Supplementary Fig. 3). This is not surprising in young stands, where biomass will largely reflect recent productivity. Canopy foliar biomass and biochemistry together drive forest productivity44 and spectra can capture signals of both^{28,32,34}. We found spectral signals of diversity-enhanced stem biomass corresponded closely with increased canopy biomass, including higher reflectance in the NIR and decreased reflectance in the SWIR. Whereas visible wavelengths are dominated by pigment absorption and SWIR wavelengths by water absorption, NIR reflectance is strongly associated with leaf, stem and canopy structure⁵⁴. Increased NIR reflectance in higher biomass stands can be attributed collectively to greater multiple scattering from mesophyll tissue at the leaf level and, at the canopy level, architectural differences including leaf and branch density and distribution, as well as total green vegetation cover and vegetation dry matter content. Decreased reflectance in the SWIR can be directly related to increased canopy water content, which scales with total foliar biomass54.

Moreover, spectral signals of diversity effects on stem biomass followed patterns of spectrally determined canopy nitrogen, connecting spectral patterns of diversity effects on stem biomass with fundamental understanding of forest productivity drivers, namely the functional link between enhanced growth and enhanced capacity to harvest light and assimilate carbon⁴⁴. Previous diversity experiments with young trees have also found that productivity is associated with community-weighted mean leaf traits including nitrogen concentration³⁶ and that enhanced biomass in mixtures compared with monocultures is associated with species identity and the dominance of fast-growing species³⁵. Our study extends these findings by showing that overall trends of positive diversity effects on stem biomass were consistent with dominance of the upper canopy by species with greater leaf nitrogen concentration (Fig. 4).

The simple partitioning approach that we present here is intended to illustrate that spectroscopic imaging can be leveraged for ecological insight. Our partitioning approach differs from previous approaches of additively partitioning the NBE into a selection or dominance effect and a complementarity effect using field measurements^{22,55,56}. These previous approaches of additive partitioning require tracking the relative biomass of species in mixture and monoculture—a seemingly intractable task with stand-scale

analyses of remotely sensed spectroscopic images which may miss species that are present in the stand but overtopped. This leads to important differences in the interpretation of spectral diversity effects. In particular, the sDE is superficially consistent with the selection²² and dominance⁵⁵ effects of previous partitions (that is, when the NBE is driven by an especially productive species). However, species interactions typically attributed to complementarity, such as partitioning light gradients⁵⁷, might affect species' dominance of the upper canopy and thus contribute to the sDE.

As a step toward spectrally identifying diversity effects in natural stands, we illustrated the potential to spectrally detect both species composition and diversity effects (Extended Data Fig. 10). Challenges remain in widely applying spectroscopic imaging to assess diversity effects, including developing models that can be applied across sensors at different spatial scales and relevant temporal scales. The models that we present here to detect biomass and species were developed with a statistical approach and calibrated onsite, and thus would require validation or further development before applying elsewhere. However, these models leverage spectral attributes directly related to canopy biomass that, in principle, ought to apply broadly, and show transferability over space and time within our study site (Supplementary Tables 2 and 3). Therefore, our findings demonstrate the potential of imaging spectroscopy to address fundamental questions about biodiversity-ecosystem function relationships while emphasizing the need to enhance the widespread applicability of models.

Spectral data lend a perspective for viewing communities, potentially opening avenues of ecological questioning and insight¹⁶. Here, we demonstrate that remote spectroscopic imaging can detect effects of diversity on stem biomass in young tree communities and provide insight into the ecological processes that drive these patterns. Crucially, the spectroscopic signal we detect is the consequence of many combined contributors (canopy architecture, chemistry, water content and species identity), and also incorporates the outcomes of biological interactions. Overall, our study highlights the promise of using remotely sensed data for testing relationships between biodiversity and ecosystem function across natural and managed ecosystems at multiple scales across the globe.

Methods

Study site. This study was conducted over 2 yr on a tree-diversity experiment that is part of the International Diversity Experiment Network with Trees (IDENT)⁴⁵. The experiment was planted in spring 2010 at the Cloquet Forestry Center (Minnesota, United States, 46° 40′ 46'′ N, 92° 31′ 12′′ W, 382 m above sea level), which has a mean annual air temperature of 4.8° C, annual precipitation of 783 mm (averaged over 1973–2008) and a short growing season of 4–5 months⁵⁸. The site is flat and was formerly forested with a sandy loam soil that was homogenized by disking before planting the experiment.

The experiment is composed of trees planted 0.4 m apart in a grid pattern to form 2.8 × 2.8 m² plots, which we refer to as stands, containing 49 trees. Stands were spaced 1 m apart. Seedlings of 12 common temperate-boreal species were planted: six from North America (Acer saccharum Marsh., Betula papyrifera Marsh., Larix laricina (Du Roi) K. Koch, Picea glauca (Moench) Voss, Pinus strobus L. and Quercus rubra L.) along with a congener of each species from Europe (Acer platanoides L., Betula pendula Roth, Larix decidua Mill., Picea abies (L.) H. Karst., Pinus sylvestris L. and Quercus robur L.). A diverse set of 48 different species assemblages was planted, namely 12 monocultures, 30 two-species mixtures and six six-species mixtures. Within an assemblage, species were planted in approximately even proportions. Each assemblage was replicated four times in a randomized block design to create a total of 192 stands. The site was fenced to exclude large herbivores and understory plants were hand-weeded regularly. Our study was conducted over 2014 and 2015 when trees were in their fifth and sixth growing seasons (mean LAI±s.d. per stand of 4.5±1.9 in the fifth and 5.9±2.6 in the sixth growing season).

Field measurements. The height and basal diameter of all trees were censused at the end of each growing season and stem biomass was estimated from these measurements with site- and species-specific allometric equations (Supplementary Table 4). Stands varied greatly in stem biomass (0.3 Mg ha⁻¹ in an *A. platanoides* monoculture to 58.8 Mg ha⁻¹ in an *A. platanoides-B. pendula* mixture in the fifth growing season and 0.6–116.4 Mg ha⁻¹ for the same assemblages in the sixth growing season).

The NBE on stem biomass (b) was calculated as follows:

$$NBE_b = b_0 - b_e \tag{1}$$

where b_o is the observed stem biomass in the mixed-species stand and b_e is the expected stem biomass, which was calculated as the sum of each constituent species' (*i*) stem biomass in monoculture (*m*) weighted by the proportion of trees of that species planted in the mixture (*p*), as follows:

$$b_{\rm e} = \sum \left(b_{m,i} \times p_i \right) \tag{2}$$

Mixed-species stands were compared with monocultures within the same experimental block. Stands varied greatly in the NBE on stem biomass (–10.9 Mg ha⁻¹ in *B. papyrifera–B. pendula* to 38.8 Mg ha⁻¹ in *A. platanoides–B. pendula* in the fifth growing season and –18.4 Mg ha⁻¹ in *P. strobus–L. laricina* to 75.8 Mg ha⁻¹ in *A. platanoides–B. pendula* in the sixth growing season), with 68% of mixed-species stands overyielding, or showing a positive NBE, in the fifth growing season and 69% in the sixth growing season.

LAI and the proportional species composition in the uppermost stratum of the canopy were determined with a line intercept approach (Supplementary Methods) on a subset of stands: 41 of the 48 species assemblages replicated across three of the four experimental blocks each year plus another five assemblages on one block in the fifth growing season. In brief, we assembled a rig to drop a line at 15 random locations within each stand during peak leaf area (August). The species identity, angle and height of each leaf intercepted by the line were recorded and subsequently used to calculate LAI (refs. ^{59,60}). The species identity of the top-most leaf intercepted by each line within a stand was used to estimate the proportional species composition in the uppermost stratum of the canopy.

Airborne data collection and processing. NASA AVIRIS-NG images of the IDENT site were acquired during the summer of the fifth growing season (25 August 2014) and the sixth growing season (30 August 2015) of the experiment. Pixels had a spatial resolution of 0.8 m and spectral resolution of approximately 5 nm with 432 bands encompassing the spectral range of 380–2,510 nm. Images were orthorectified, radiometrically calibrated and atmospherically corrected to apparent surface reflectance by the Jet Propulsion Laboratory. Noisy and water absorption bands were excluded and the remaining spectral regions (416.4–1,343, 1,463.2–1,733.7, 1,768.7–1,803.8 and 1,984.1–2,399.8 nm) were used for analyses.

To match spectra to stands, we created shape files of the stand locations by manually delineating polygons on the spectroscopic images (Supplementary Fig. 4). One shape file was created for each year's image as the images did not perfectly align. False colour images were used to visualize the boundaries of stands and the known size and distance among stands was used as a guide. These shape files were used to extract the pixels occurring within each stand. Pixels were extracted if their centre was located within the stand boundary; this means that some pixels that extended over the stand boundary were spectrally mixed with the matrix between stands. To calculate stand-level mean spectra, we weighted the edge pixels by the proportion of each pixel occurring within the stand boundary.

Spectral detection of biomass and diversity effects on biomass. We used stand-level mean spectra (averaged across the pixels within a stand using the pixels weighted by proportion within the stand boundary) to predict stem biomass using PLSR (ref. 61) on the full spectrum, minus noisy and water absorption bands. To maximize the generality of the PLSR model across acquisitions that may have varied in overall scene brightness, one model was developed using vector-normalized spectra and field-measured stem biomass from both growing seasons. We followed the PLSR procedure outlined by Serbin et al.⁶² whereby data were split into a calibration (75%) and an independent validation subset (25%). Subsets were sampled in a stratified random fashion to evenly represent growing seasons and ensure that each subset encompassed the range of observed values for stem biomass that we were predicting. We further split the calibration subset, resampling 80% of these data without replacement (in jackknife fashion) 1,000 times again in the same stratified random fashion. For each of these 1,000 iterations, we fitted a PLSR model with the pls package⁶³ in R (ref. ⁶⁴). To avoid potential overfitting of models, the optimal number of PLSR components was chosen as the number where adding more components did not significantly reduce the predicted residual sum of squares (PRESS) on average across the 1,000 iterations; this was assessed with t-tests. We assessed model fit by calculating the coefficient of determination (R2), r.m.s.e., relative r.m.s.e. (%r.m.s.e., calculated as r.m.s.e./range of data) and bias of the relationship between the stem biomass measured on stands and the mean values of stem biomass predicted for stands within the calibration, cross-validation and independent validation data subsets. Wavelengths of importance were extracted for each model iteration using the varImp function in the caret package65 in R, which assesses how much the wavelength reduces the sums of squares of the model fit. As a baseline to compare with the performance of the PLSR model of stem biomass, we also calculated a common index of vegetation cover—the NDVI (ref. 66). We calculated NDVI as $(R_{800} - R_{680})/(R_{800} + R_{680})$, where R_{800} and R_{680} are the weighted stand average AVIRIS-NG reflectances at 800 and 680 nm, respectively.

We tested the capacity to detect the NBE on stem biomass using spectra. We also partitioned the spectrally detected NBE on stem biomass into the spectral dominance and plasticity effects on stem biomass. To calculate these diversity effects, we simulated the spectra of mixed-species stands using pixels from monoculture stands (Fig. 1), which required knowing the composition of mixed-species stands. We ran two simulations with each simulation repeated 1,000 times. First, for each mixed-species stand, we drew pixels from monocultures according to the proportion of trees (T) per species that were planted in the mixed-species stand (Sim_T). By drawing trees according the proportion of trees planted (rather than alive at the time of sampling), this treats differences in mortality between monocultures and mixtures as part of the diversity or mixing effect. In the calculation of diversity effects, each block was treated separately, such that simulations for each mixed-species stand drew pixels from the monocultures present on the same block. Second, we drew pixels from monocultures according to the relative proportion of leaves (L) in the uppermost stratum of the canopy that belonged to each species (Sim_L). This simulation was assessed for the subset of stands where the proportional species composition in the upper stratum of the canopy was estimated in the field.

To calculate spectral diversity effects on stem biomass, we applied the coefficients from each of the 1,000 iterations of the PLSR model of stem biomass to (1) the stand-level mean observed spectrum of each stand (Obs) to estimate the stem biomass observed in each mixed-species stand and (2) to the stand-level mean simulated spectra (Sim_T and Sim_L) of each stand to estimate the stem biomass expected in the mixture based on monocultures if the relative species composition of the upper canopy matched the relative proportion of stems per species (Sim_T), or matched the relative proportion of leaves per species (Sim_L). The stem biomass values predicted from the observed spectrum minus the values predicted from Sim_T were considered our measure of the spectrally predicted NBE (sNBE) on biomass. The difference in predicted stem biomass between Sim_T and Sim_L represented the observed spectrum and Sim_L represented the sPE on stem biomass (Fig. 1).

Mapping canopy nitrogen concentration. We followed the procedure outlined in Singh et al.²⁹ to map canopy nitrogen concentration from AVIRIS-NG imagery. We measured full-range (400-2,500 nm) reflectance on fresh leaves (or mat of needles) of three trees per species in each of 36 stands within one block in the fifth growing season and in 39 stands within two blocks in the sixth growing season with an ASD FieldSpec 3 spectroradiometer (Analytical Spectral Devices). For each tree, we measured three leaves from each of the top, middle and bottom of the crown. Leaf-level nitrogen concentration (N_{mass}, %) was estimated using leaf-level spectra with pre-existing leaf-level PLSR models ($R^2 = 0.95$) (ref. 67). For each tree, the nitrogen predictions of the three replicate leaves per crown layer were averaged to obtain the nitrogen concentration per crown layer and these nitrogen values per crown layer were used to calculate a weighted mean estimate of leaf nitrogen per tree, with the top of crown nitrogen value weighted as 90%, middle of crown value as 9% and bottom of crown value as 1%. For each species per stand, the weighted mean leaf nitrogen per tree from the three sampled trees were averaged to give the species' mean leaf nitrogen per stand. The species' mean nitrogen per stand were upscaled to stand-level nitrogen concentration by using LAI estimated per species per stand from field-based measurements (Supplementary Methods) to infer species' relative abundance; gaps in data, where LAI or leaf-level spectra was not sampled for a stand, were infilled using data from species growing in the same assemblage on another block where possible or, if not, using site level means for each species' LAI and nitrogen. A canopy-level PLSR model was developed from stand-level nitrogen and stand-level spectra to predict canopy nitrogen in both years (independent validation: $R^2 = 0.78$, r.m.s.e. = 0.17, %r.m.s.e. = 12.4%). This model was applied across all pixels in the AVIRIS-NG images of the experiment in the fifth and sixth growing seasons (Extended Data Fig. 5). Predicted nitrogen values were subsequently averaged to give a mean value for each stand and growing season, again weighting pixels by their proportional area within the stand boundary. This approach estimates canopy nitrogen weighted toward the nitrogen concentration of the upper canopy, which matches the portion of the canopy sensed by AVIRIS-NG and is the most important tree layer functionally in terms of carbon assimilation.

We compared spectrally predicted canopy nitrogen with canopy nitrogen based on field measurements. For each species, we destructively sampled one to three mature leaves (fascicles or branchlets for needle-leafed species) from near the top of the crown of each of three trees chosen at random within each monoculture stand (one stand per block, n=4). Samples were collected in late July during the fourth growing season. Leaves were pooled to give one sample per species per block, finely ground (lamina only), analysed for total nitrogen at the University of Nebraska, Lincoln, using a Costech ECS 4010 element analyser, expressed as a percentage of leaf mass (N_{mass}, %) and averaged to give one value per species. Canopy-level nitrogen from these field measurements was calculated for each stand by weighting species' nitrogen values by species' relative LAI in mixed-species plots; gaps in LAI data were infilled as described above for the spectral mapping of canopy nitrogen.

Spectral diversity effects on spectrally predicted canopy nitrogen were calculated with a similar approach as for stem biomass except, when simulating mixtures from monocultures (Fig. 1), the spectral estimates of canopy nitrogen for pixels were drawn from monoculture stands.

An approach using only spectra: spectrally identifying species composition for the analysis of diversity effects on biomass. As a step toward an approach for identifying spectral diversity effects in naturally assembled forests where the species composition of stands may be unknown, we assessed whether we could first use spectra to identify the species composition of stands and then use these spectrally identified species compositions in combination with spectrally predicted stem biomass to calculate spectral diversity effects on stem biomass. Partial least squares discriminant analysis (PLS-DA) (ref. 63) was used to develop a model to distinguish among the 12 species on the basis of spectra drawn from monoculture stands across both growing seasons. Using pixels at their original resolution from the 48 monoculture stands (four stands of each of the 12 species; 9–14 pixels per stand with a mean of 12 pixels), we vector-normalized spectra and split data into calibration (50%) and validation (50%) subsets stratified by species, experimental blocks and growing seasons. Data were resampled without replacement, evenly drawing from species, experimental blocks and growing seasons, 300 times and a PLS-DA model was fitted to each sample with the pls package. The number of components (23) was chosen by assessing kappa scores for iterative model runs with increasing numbers of components (Supplementary Fig. 5).

For each growing season, coefficients from the resulting 300 PLS-DA iterations were applied to predict the species composition of stands and to simulate the spectra of mixtures from monocultures. For each pixel, we calculated the fraction of the 300 PLS-DA iterations assigned to each of the 12 species. We then took the average of these fractional species assignments across all pixels within a stand as our estimate of the proportional species composition on a stand (Extended Data Fig. 8). Monocultures were spectrally assigned by assuming that each block contained one monoculture stand per species. The monoculture of a given species was assumed to be the stand with the greatest proportion of pixels assigned to that species; in the case of a tie, more than one stand was treated as the monoculture and we took the mean across these spectra (this was the case for some stands dominated by *Betula* spp.). All other stands were assumed to be mixed-species stands.

We simulated the spectra of mixed-species stands from the spectrally assigned monocultures (above) using two approaches that approximately correspond to the simulations based on the proportion of trees (Sim_T) and the proportion of the upper stratum of the canopy (Sim_L) (Fig. 1). Traditional field-based approaches of assessing diversity effects on productivity²² require knowing initial proportion of species planted or seeded. However, initial proportions cannot be spectrally determined. Instead, for our first approach, we simulated an 'equal abundance' scenario—an analogue of Sim,—that requires no prior knowledge but makes the assumption that all species spectrally identified as present within the canopy of a mixed-species stand have equal abundance in that stand (Sim_{sID(T)}). This approximates the design of the tree-diversity experiment and is analogous to assuming demographic equivalence among tree species. In the second approach—an analogue of Sim_L—we took a weighted mean from the stand-level mean spectra of spectrally assigned monocultures; spectra were weighted according to the spectrally determined proportional composition of stands, which presumably represents their proportional abundance in the upper stratum of the canopy (Sim_{sID(L)}). Finally, we applied the PLSR models of stem biomass to the observed spectrum (Obs) as well as the two simulated spectra ($\mathrm{Sim}_{\mathrm{sID(T)}}$ and $\mathrm{Sim}_{\mathrm{sID(L)}}$) for each stand. Following our earlier approach (Fig. 1), the difference between biomass estimated from the observed spectrum and Sim_{siD(T)} represents the NBE (sNBE_{siD}) on biomass, while the difference between $Sim_{sID(T)}$ and $Sim_{sID(L)}$ represents the sDE on biomass (sDE_{siD}) and between the observed spectrum and $Sim_{siD(L)}$ represents the sPE on biomass (sPE_{sID}).

Reporting Summary. Further information on research design is available in the Nature Research Reporting Summary linked to this article.

Data availability

AVIRIS-NG data can be downloaded from https://aviris-ng.jpl.nasa.gov/alt_locator/. Image level spectra, canopy nitrogen predictions and field-based measurements along with coefficients for PLSR and PLS-DA models are available on the Data Repository for the University of Minnesota⁶⁸ (https://doi.org/10.13020/s7pf-am91).

Code availability

Code for the PLSR and PLS-DA models developed here along with code for simulating spectra, applying PLSR models and calculating spectral diversity effects are available at the Data Repository for the University of Minnesota 68 (https://doi.org/10.13020/s7pf-am91).

Received: 26 January 2020; Accepted: 9 September 2020; Published online: 2 November 2020

References

- Pimm, S. L. et al. The biodiversity of species and their rates of extinction, distribution, and protection. Science 344, 1246752 (2014).
- Isbell, F. et al. Linking the influence and dependence of people on biodiversity across scales. *Nature* 546, 65–72 (2017).

- 3. Gonzalez, A. et al. Scaling-up biodiversity–ecosystem functioning research. *Ecol. Lett.* **23**, 757–776 (2020).
- Chase, J. M. et al. Species richness change across spatial scales. Oikos 128, 1079–1091 (2019).
- Tilman, D., Isbell, F. & Cowles, J. M. Biodiversity and ecosystem functioning. Annu. Rev. Ecol. Evol. Syst. 45, 471–493 (2014).
- Summary for Policymakers of the Global Assessment Report on Biodiversity and Ecosystem Services (eds Díaz, S. et al.) (IPBES, 2019).
- Cardinale, B. J. et al. The functional role of producer diversity in ecosystems. Am. J. Bot. 98, 572–592 (2011).
- Thompson, P. L., Isbell, F., Loreau, M., O'Connor, M. I. & Gonzalez, A. The strength of the biodiversity–ecosystem function relationship depends on spatial scale. *Proc. R. Soc. B* 285, 20180038 (2018).
- Barry, K. E. et al. A universal scaling method for biodiversity-ecosystem functioning relationships. Preprint at bioRxiv https://doi.org/10.1101/662783 (2019)
- O'Connor, M. I. et al. A general biodiversity-function relationship is mediated by trophic level. Oikos 126, 18–31 (2017).
- Oehri, J., Schmid, B., Schaepman-Strub, G. & Niklaus, P. A. Biodiversity promotes primary productivity and growing season lengthening at the landscape scale. *Proc. Natl Acad. Sci. USA* 114, 10160–10165 (2017).
- Duffy, J. E., Godwin, C. M. & Cardinale, B. J. Biodiversity effects in the wild are common and as strong as key drivers of productivity. *Nature* 549, 261–264 (2017).
- Liang, J. et al. Positive biodiversity-productivity relationship predominant in global forests. Science 354, aaf8957 (2016).
- Chisholm, R. A. et al. Scale-dependent relationships between tree species richness and ecosystem function in forests. *J. Ecol.* 101, 1214–1224 (2013).
- Jetz, W. et al. Monitoring plant functional diversity from space. Nat. Plants 2, 16024 (2016).
- Cavender-Bares, J. et al. Harnessing plant spectra to integrate the biodiversity sciences across biological and spatial scales. Am. J. Bot. 104, 966–969 (2017).
- Asner, G. P. & Martin, R. E. Airborne spectranomics: mapping canopy chemical and taxonomic diversity in tropical forests. Front. Ecol. Environ. 7, 269–276 (2009).
- 18. Climate Change and Land (eds Shukla, P. R. et al.) (IPCC, in the press).
- 19. Fernández, N., Ferrier, S., Navarro, L. M. & Pereira, H. M. in Remote Sensing of Plant Biodiversity (eds Cavender-Bares, J. et al.) 485-501 (Springer, 2020).
- Cavender-Bares, J., Schweiger, A. K., Pinto-Ledezma, J. N. & Meireles, J. E. in Remote Sensing of Plant Biodiversity (eds Cavender-Bares, J. et al.) 13–42 (Springer, 2020).
- 21. Strategic Plan for Biodiversity 2011–2020, including Aichi Biodiversity Targets (Convention on Biological Diversity, 2010).
- Loreau, M. & Hector, A. Partitioning selection and complementarity in biodiversity experiments. *Nature* 412, 72–76 (2001).
- 23. Schimel, D., Schneider, F. D., Carbon, J. P. L. & Ecosystem, P. Flux towers in the sky: global ecology from space. *New Phytol.* **224**, 570–584 (2019).
- Féret, J.-B. & Asner, G. P. Mapping tropical forest canopy diversity using high-fidelity imaging spectroscopy. *Ecol. Appl.* 24, 1289–1296 (2014).
- Schneider, F. D. et al. Mapping functional diversity from remotely sensed morphological and physiological forest traits. Nat. Commun. 8, 1441 (2017).
- Gholizadeh, H. et al. Remote sensing of biodiversity: soil correction and data dimension reduction methods improve assessment of α-diversity (species richness) in prairie ecosystems. *Remote Sens. Environ.* 206, 240–253 (2018).
- 27. Wang, R. & Gamon, J. A. Remote sensing of terrestrial plant biodiversity. *Remote Sens. Environ.* **231**, 111218 (2019).
- Ollinger, S. V. et al. Canopy nitrogen, carbon assimilation, and albedo in temperate and boreal forests: functional relations and potential climate feedbacks. *Proc. Natl Acad. Sci. USA* 105, 19335–19340 (2008).
- Singh, A., Serbin, S. P., McNeil, B. E., Kingdon, C. C. & Townsend, P. A. Imaging spectroscopy algorithms for mapping canopy foliar chemical and morphological traits and their uncertainties. *Ecol. Appl.* 25, 2180–2197 (2015).
- Ustin, S. L., Roberts, D. A., Gamon, J. A., Asner, G. P. & Green, R. O. Using imaging spectroscopy to study ecosystem processes and properties. *BioScience* 54, 523–534 (2004).
- Fallon, B. et al. Spectral differentiation of oak wilt from foliar fungal disease and drought is correlated with physiological changes. *Tree Physiol.* 40, 377–390 (2020).
- Schweiger, A. K. et al. Using imaging spectroscopy to predict above-ground plant biomass in alpine grasslands grazed by large ungulates. J. Veg. Sci. 26, 175–190 (2015).
- Caughlin, T. T. et al. A hyperspectral image can predict tropical tree growth rates in single-species stands. Ecol. Appl. 26, 2369–2375 (2016).
- Serbin, S. P. et al. Remotely estimating photosynthetic capacity, and its response to temperature, in vegetation canopies using imaging spectroscopy. *Remote Sens. Environ.* 167, 78–87 (2015).
- 35. Tobner, C. M. et al. Functional identity is the main driver of diversity effects in young tree communities. *Ecol. Lett.* **19**, 638–647 (2016).

- Grossman, J. J., Cavender-Bares, J., Hobbie, S. E., Reich, P. B. & Montgomery, R. A. Species richness and traits predict overyielding in stem growth in an early-successional tree diversity experiment. *Ecology* 98, 2601–2614 (2017).
- Sapijanskas, J., Paquette, A., Potvin, C., Kunert, N. & Loreau, M. Tropical tree diversity enhances light capture through crown plasticity and spatial and temporal niche differences. *Ecology* 95, 2479–2492 (2014).
- 38. Niklaus, P. A., Baruffol, M., He, J. S., Ma, K. & Schmid, B. Can niche plasticity promote biodiversity–productivity relationships through increased complementarity? *Ecology* **98**, 1104–1116 (2017).
- Williams, L. J., Paquette, A., Cavender-Bares, J., Messier, C. & Reich, P. B. Spatial complementarity in tree crowns explains overyielding in species mixtures. *Nat. Ecol. Evol.* 1, 0063 (2017).
- Forrester, D. I. & Bauhus, J. A review of processes behind diversityproductivity relationships in forests. Curr. For. Rep. 2, 45–61 (2016).
- Jactel, H. et al. Tree diversity drives forest stand resistance to natural disturbances. Curr. For. Rep. 3, 223–243 (2017).
- Wright, A. J., Wardle, D. A., Callaway, R. M. & Gaxiola, A. The overlooked role of facilitation in biodiversity experiments. *Trends Ecol. Evol.* 32, 383–390 (2017).
- Kothari, S., Montgomery, R. & Cavender-Bares, J. Physiological responses to light explain competition and facilitation in a tree diversity experiment. Preprint at bioRxiv https://doi.org/10.1101/845701 (2020).
- 44. Reich, P. B. Key canopy traits drive forest productivity. Proc. R. Soc. B 279, 2128-2134 (2012).
- Tobner, C. M., Paquette, A., Reich, P. B., Gravel, D. & Messier, C. Advancing biodiversity–ecosystem functioning science using high-density tree-based experiments over functional diversity gradients. *Oecologia* 174, 609–621 (2014).
- Schweiger, A. K. et al. Plant spectral diversity integrates functional and phylogenetic components of biodiversity and predicts ecosystem function. *Nat. Ecol. Evol.* 2, 976–982 (2018).
- 47. Reich, P. B. et al. Impacts of biodiversity loss escalate through time as redundancy fades. *Science* **336**, 589–592 (2012).
- 48. Reich, P. B. The world-wide 'fast-slow'plant economics spectrum: a traits manifesto. *J. Ecol.* **102**, 275–301 (2014).
- Williams, L. J., Cavender-Bares, J., Paquette, A., Messier, C. & Reich, P. B. Light mediates the relationship between community diversity and trait plasticity in functionally and phylogenetically diverse tree mixtures. *J. Ecol.* 108, 1617–1634 (2020).
- Huete, A. R., Liu, H. & van Leeuwen, W. J. D. The use of vegetation indices in forested regions: issues of linearity and saturation. *IEEE Trans. Geosci. Remote Sens.* 4, 1966–1968 (1997).
- Tjoelker, M. G., Volin, J. C., Oleksyn, J. & Reich, P. B. Interaction of ozone pollution and light effects on photosynthesis in a forest canopy experiment. *Plant Cell Environ.* 18, 895–905 (1995).
- Pacala, S. W. et al. Forest models defined by field measurements: estimation, error analysis and dynamics. *Ecol. Monogr.* 66, 1–43 (1996).
- 53. Reich, P. B., Ellsworth, D. S., Kloeppel, B. D., Fownes, J. H. & Gower, S. T. Vertical variation in canopy structure and CO₂ exchange of oak–maple forests: influence of ozone, nitrogen, and other factors on simulated canopy carbon gain. *Tree Physiol.* 7, 329–345 (1990).
- Ollinger, S. V. Sources of variability in canopy reflectance and the convergent properties of plants. New Phytol. 189, 375–394 (2011).
- Fox, J. W. Interpreting the 'selection effect' of biodiversity on ecosystem function. Ecol. Lett. 8, 846–856 (2005).
- Isbell, F. et al. Quantifying effects of biodiversity on ecosystem functioning across times and places. Ecol. Lett. 21, 763–778 (2018).
- Barry, K. E. et al. The future of complementarity: disentangling causes from consequences. *Trends Ecol. Evol.* 34, 167–180 (2019).
- Reich, P. B. et al. Geographic range predicts photosynthetic and growth response to warming in co-occurring tree species. Nat. Clim. Change 5, 148–152 (2015).
- Thomas, S. C. & Winner, W. E. Leaf area index of an old-growth Douglas-fir forest estimated from direct structural measurements in the canopy. *Can. J. Res.* 30, 1922–1930 (2000).
- Nock, C. A., Caspersen, J. P. & Thomas, S. C. Large ontogenetic declines in intra-crown leaf area index in two temperate deciduous tree species. *Ecology* 89, 744–753 (2008).
- Wold, S., Sjöström, M. & Eriksson, L. PLS-regression: a basic tool of chemometrics. Chemom. Intell. Lab. Syst. 58, 109–130 (2001).
- Serbin, S. P., Singh, A., McNeil, B. E., Kingdon, C. C. & Townsend, P. A. Spectroscopic determination of leaf morphological and biochemical traits for northern temperate and boreal tree species. *Ecol. Appl.* 24, 1651–1669 (2014).
- Mevik, B.-H., Wehrens, R. & Liland, K. H. pls: Partial least squares and principal component regression. R package version 2.7.0 https:// CRAN.R-project.org/package=pls (2018).
- 64. R Core Team R: A Language and Environment for Statistical Computing (R Foundation for Statistical Computing, 2018).
- Kuhn, M. caret: Classification and regression training. R package version 6.0.81 https://CRAN.R-project.org/package=caret (2018).

- Tucker, C. J. Red and photographic infrared linear combinations for monitoring vegetation. *Remote Sens. Environ.* 8, 127–150 (1979).
- 67. Serbin, S. P. Spectroscopic Determination of Leaf Nutritional, Morphological, and Metabolic Traits. PhD thesis, Univ. of Wisconsin-Madison (2012).
- Williams, L. J. et al. Data and Code for Remote Spectral Detection of Biodiversity Effects on Forest Biomass (Data Repository for the University of Minnesota, 2020); https://doi.org/10.13020/s7pf-am91

Acknowledgements

We thank K. Rice, R. Bermudez, J. Gamon, A. Mazur, A. Schweiger, M. Sinnen, R. Wang and numerous interns for field assistance. We also thank E. Butler, J. Ditmer, B. Fallon, S. Hobbie, F. Isbell, S. Kothari, J. E. Meireles, R. Putnam, G. Sapes and A. Schweiger for comments. The project was funded by a National Science Foundation and National Aeronautic and Space Administration grant awarded to J.C.-B. (grant no. DEB-1342872) and P.A.T. (grant no. DEB-1342778) through the Dimensions of Biodiversity program, the Hubachek Wilderness Research endowment (University of Minnesota), the Canada Research Chairs program and the National Science Foundation's Biology Integration Institutes program (grant no. NSF-DBI-2021898).

Author contributions

This work is part of the Dimensions of Biodiversity project 'Linking remotely sensed optical diversity to genetic, phylogenetic and functional diversity to predict ecosystem

processes', conceptualized by J.C.-B. and P.A.T. J.C.-B. and L.J.W. conceptualized this study. P.B.R., C.M. and A.S. designed and implemented the broader IDENT study. J.J.C., A.S. and L.J.W. collected data. Z.W. prepared spectral data and mapped canopy nitrogen. L.J.W. analysed the data with assistance from J.C.-B., J.J.C. and Z.W. L.J.W. wrote the first draft of the manuscript. All authors contributed to revisions and further manuscript development.

Competing interests

The authors declare no competing interests.

Additional information

Extended data is available for this paper at https://doi.org/10.1038/s41559-020-01329-4. **Supplementary information** is available for this paper at https://doi.org/10.1038/s41559-020-01329-4.

Correspondence and requests for materials should be addressed to L.J.W. or J.C.-B.

Peer review information Peer reviewer reports are available.

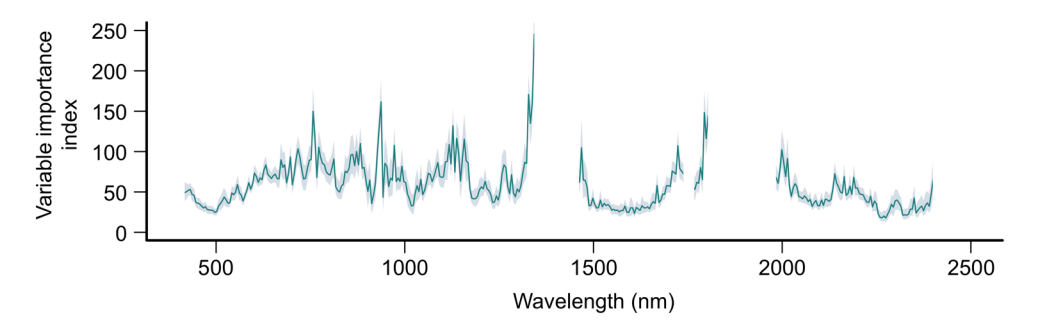
Reprints and permissions information is available at www.nature.com/reprints.

Publisher's note Springer Nature remains neutral with regard to jurisdictional claims in published maps and institutional affiliations.

© The Author(s), under exclusive licence to Springer Nature Limited 2020

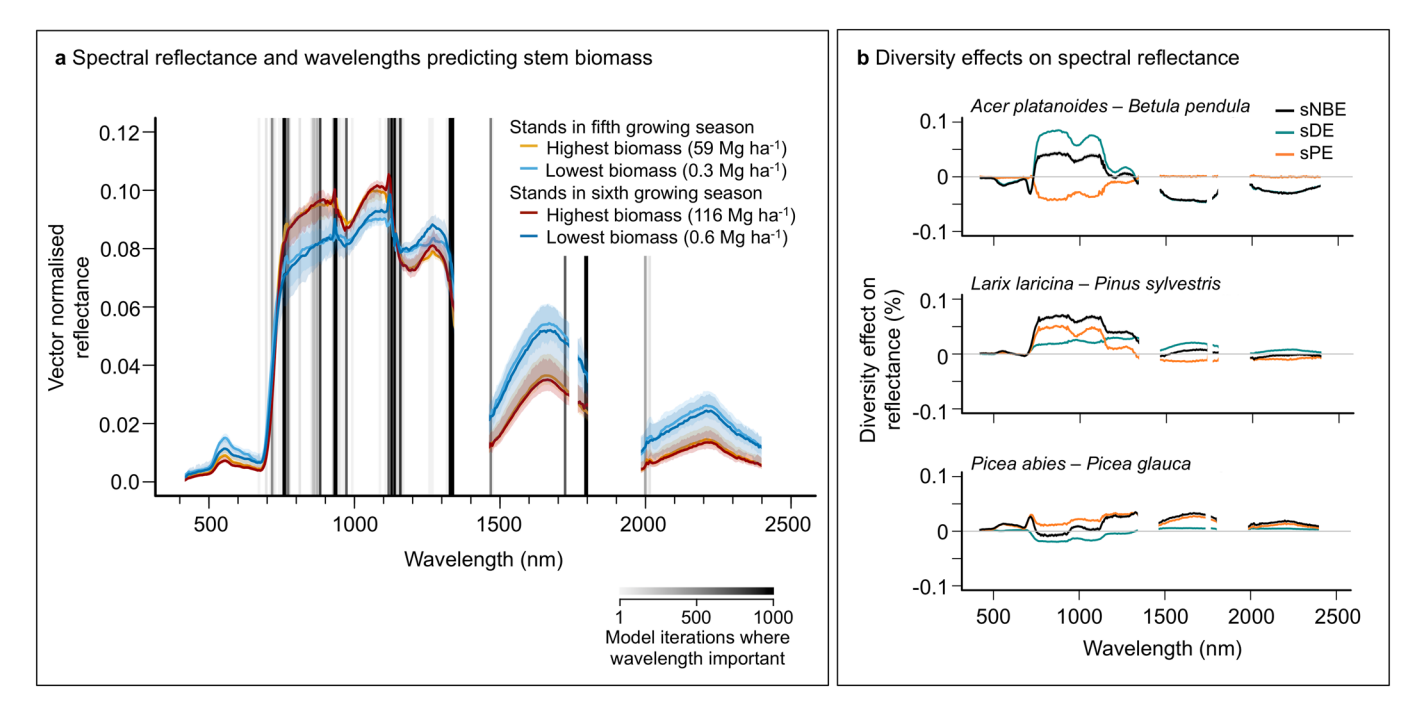
Data subset	R^2	r.m.s.e.	% r.m.s.e.	bias	Р	n	n. comp.
Cal.	0.96	2.15	1.9	0.00	<0.001	232	13
Val.	0.97	1.52	1.3	0.11	<0.001	56	
Ind. val.	0.91	6.07	6.3	0.20	<0.001	96	

Extended Data Fig. 1 | Fits of the PLSR model of stem biomass. Partial least squares regression (PLSR) model combining data from the fifth and sixth growing seasons, showing fits for calibration (Cal.), cross-validation (Val.) and independent validation (Ind. val.) data subsets. Spectra were vector-normalized. n = number of stands, n comp. = number of components in model.

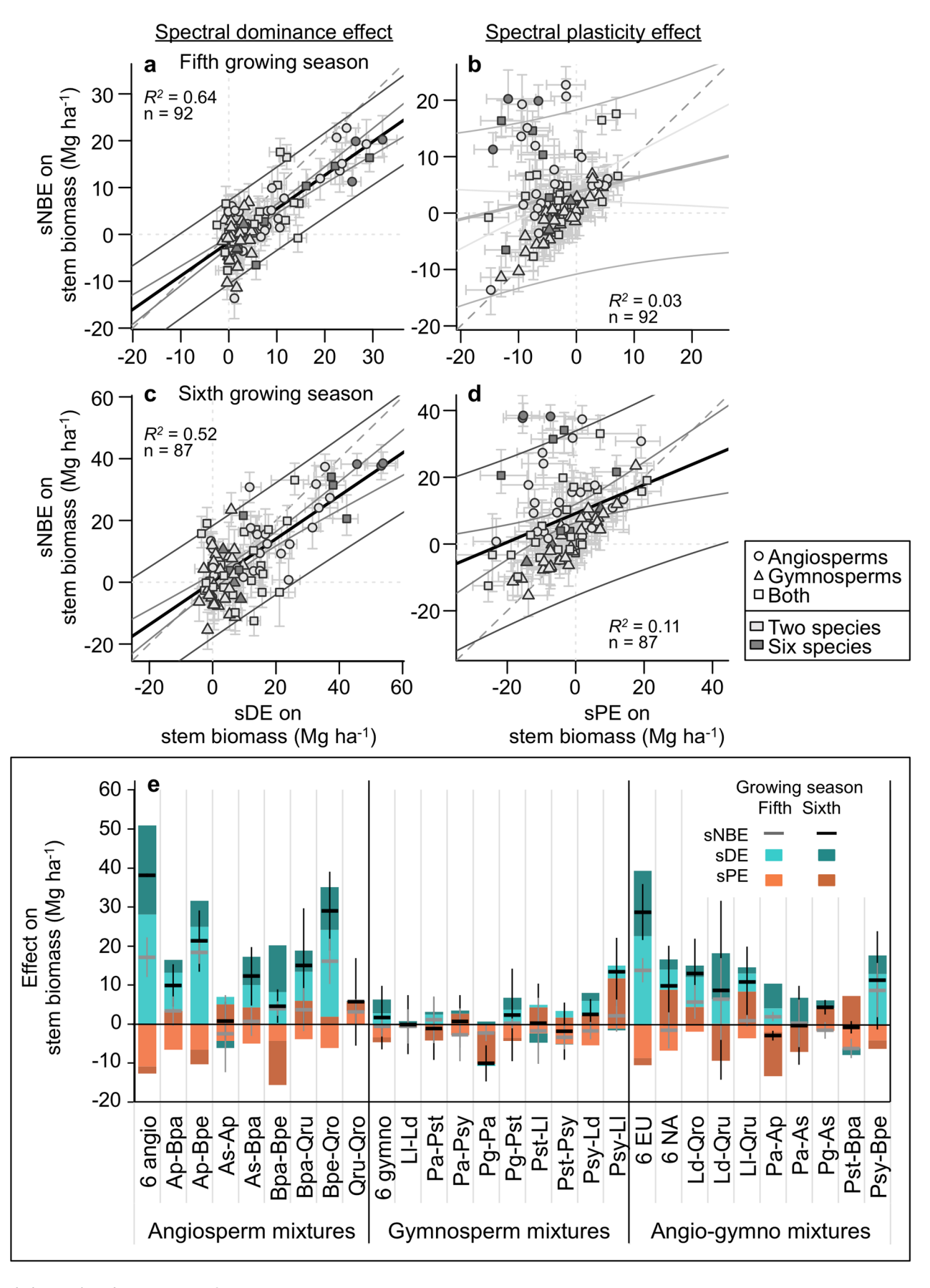


Extended Data Fig. 2 | Wavelengths of importance in the PLSR model of stem biomass. The variable importance index represents the reduction of sums of squares⁶³. Solid line indicates the mean and shading indicates the 95% confidence intervals around the mean importance value for each wavelength across the 1000 model iterations. Noisy and water absorption wavelengths are omitted.

NATURE ECOLOGY & EVOLUTION ARTICLES



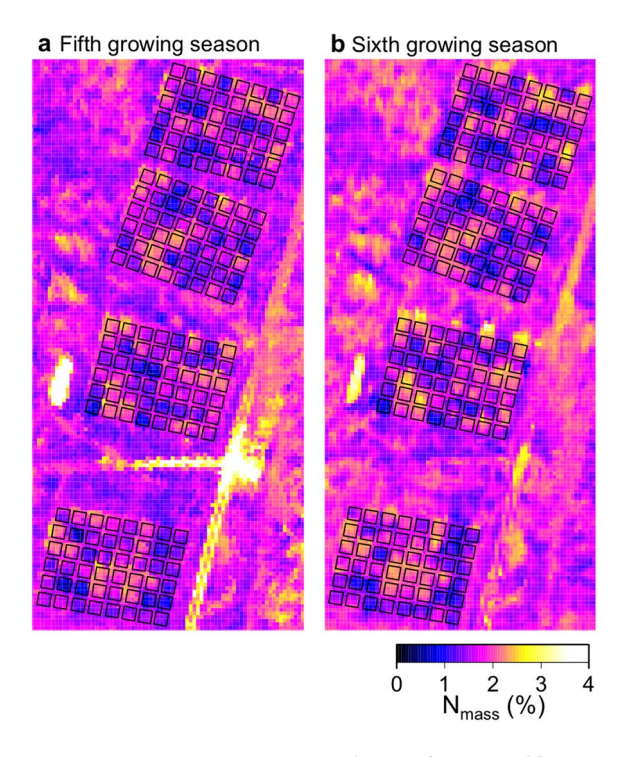
Extended Data Fig. 3 | Examples of spectral reflectance and diversity effects on spectral reflectance. a, Spectral reflectance of four stands, representing the range in stem biomass in each growing season, and important wavelengths in the PLSR model of stem biomass. Important wavelengths (number of iterations where the wavelength was among the 20 most important based on the reduction of the sums of squares⁵³) are indicated with the intensity of vertical lines. Shading around spectra indicates 95% confidence intervals among pixels within stands. b, Examples of diversity effects on the spectral reflectance of stands, showing the difference between observed spectral reflectance (Obs) and simulated spectral reflectance (Sim_T) (that is, the spectral net biodiversity effect, sNBE) separated into the additive contributions of spectral dominance (sDE) and spectral plasticity (sPE) (see Fig. 1). These stands are from the fifth growing season and illustrate strongly positive, moderately positive, and negative field-measured NBE on stem biomass (top to bottom panels, respectively). Noisy and water absorption wavelengths are omitted.



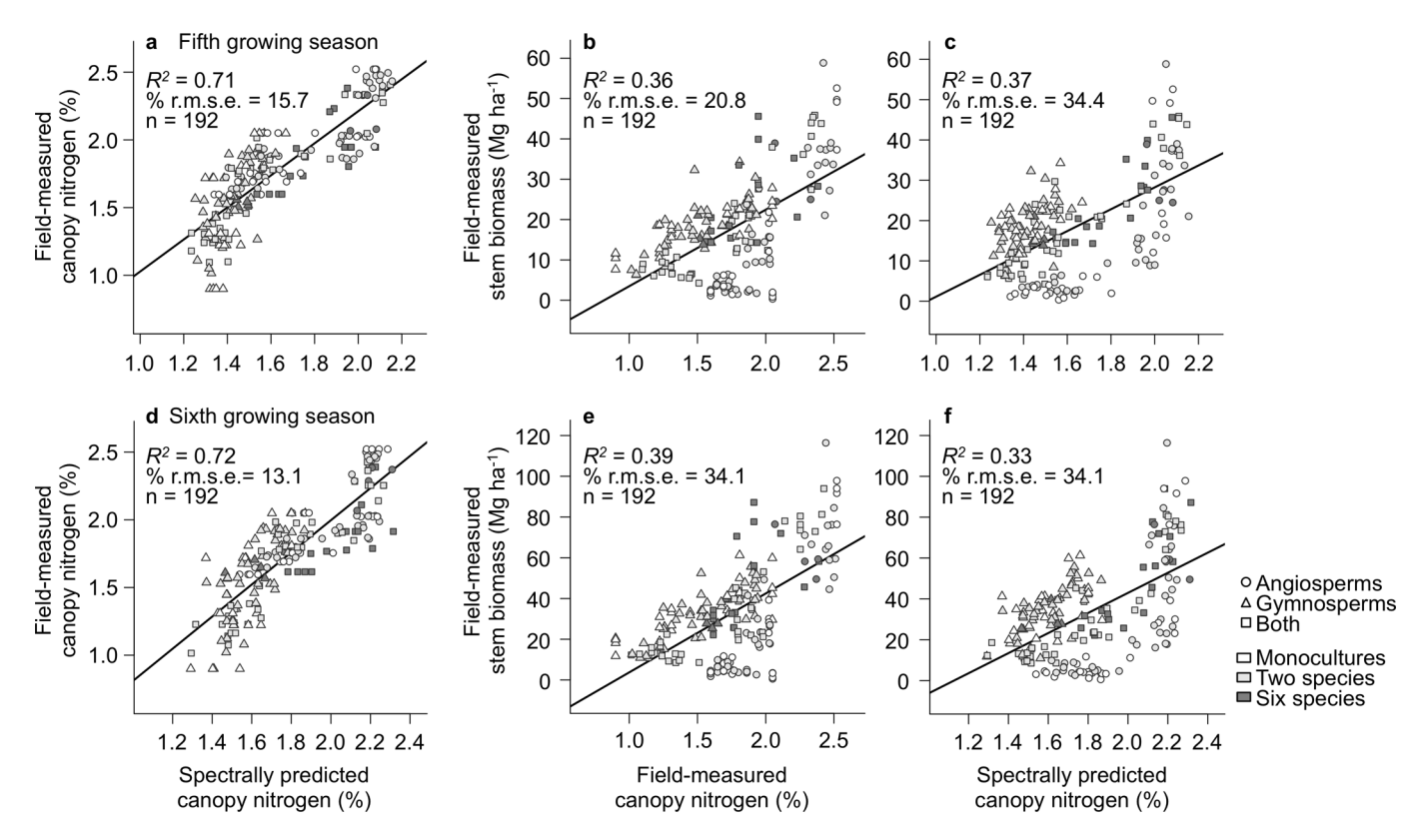
Extended Data Fig. 4 | See next page for caption.

NATURE ECOLOGY & EVOLUTION ARTICLES

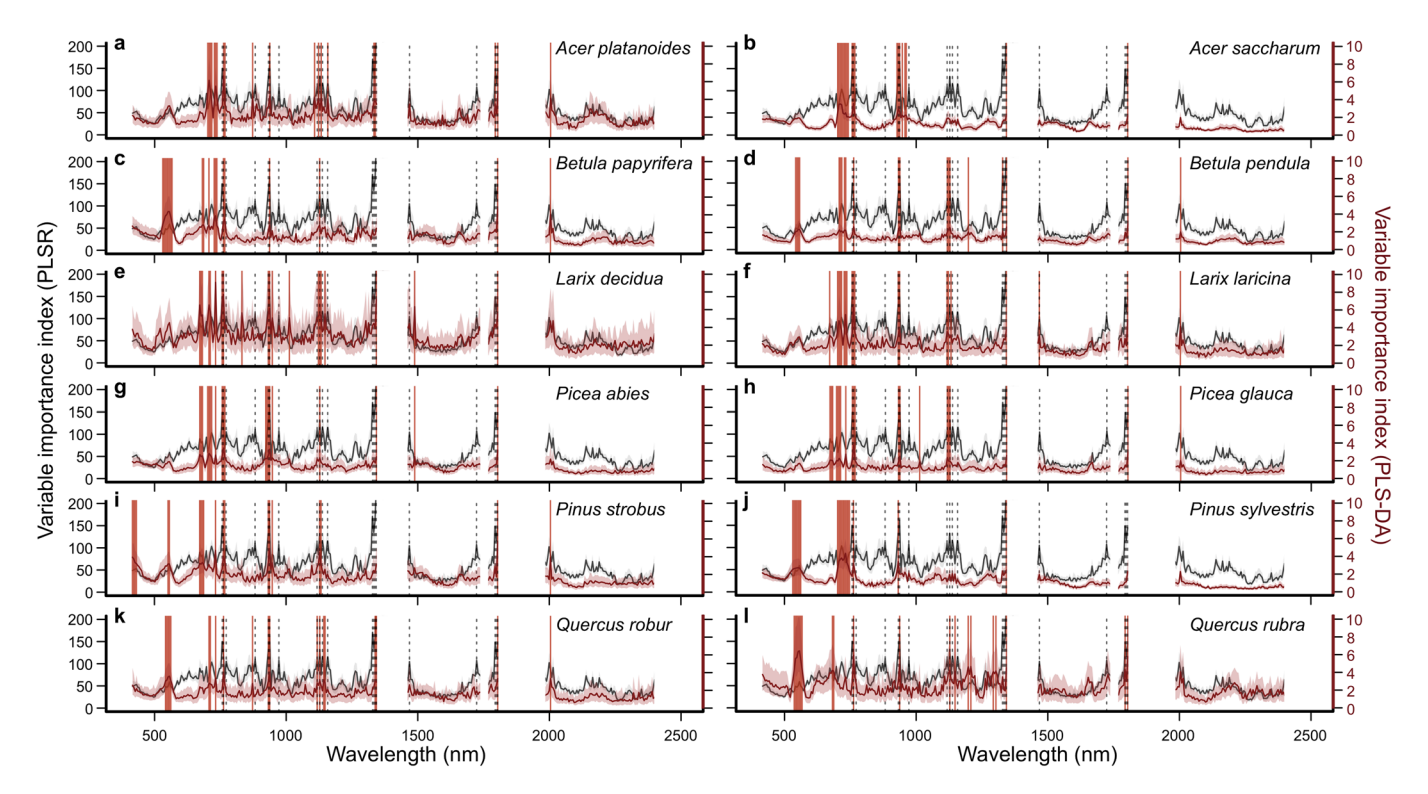
Extended Data Fig. 4 | Spectrally determined diversity effects on stem biomass and the spectral net biodiversity effect. Contributions of the spectral dominance effect (sDE) (\mathbf{a} , \mathbf{c}) and spectral plasticity effect (sPE) (\mathbf{b} , \mathbf{d}) on stem biomass to the spectrally predicted net biodiversity effect (sNBE) on stem biomass in the fifth (\mathbf{a} , \mathbf{b}) and sixth (\mathbf{c} , \mathbf{d}) growing seasons. Error bars show 95% confidence intervals among the 1000 model iterations. Thick line represents the regression line (significant for sDE in both years and sPE in the fifth growing season, $P \le 0.002$, but not for sPE in the sixth growing season, P = 0.117). Dark grey lines represent the 95% prediction interval and light grey lines the 95% confidence interval of the models. Dashed grey line shows 1:1. \mathbf{e} , Mean contributions of sDE and sPE on stem biomass to sNBE on stem biomass for each species mixture, showing effects in the fifth growing season and the increase (or decrease) in effects in the sixth growing season. Error bars for sNBE represent standard deviations among blocks (n = 3; an additional five mixed-species stands measured in one block in the fifth growing season are omitted). 6 NA = all six species of North American origin, 6 EU = all six species of European origin, 6 angio = all six angiosperms, 6 gymno = all six gymnosperms, Ap = Acer platanoides, As = Acer saccharum, Bpa = Betula papyrifera, Bpe = Betula pendula, Ld = Larix decidua, Ll = Larix laricina, Pa = Picea abies, Pg = Picea glauca, Pst = Pinus strobus, Psy = Pinus sylvestris, Qro = Quercus robur and Qru = Quercus rubra.



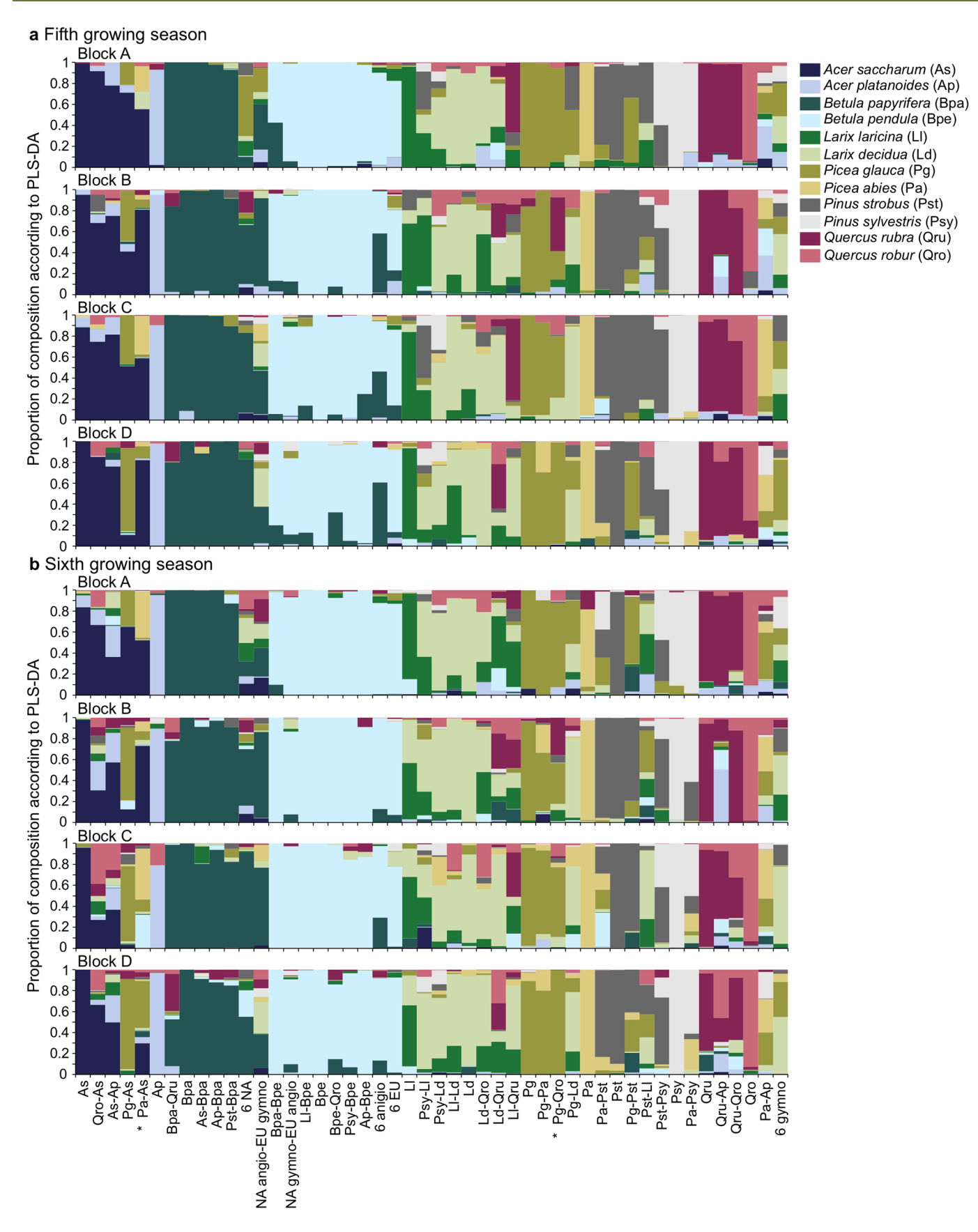
Extended Data Fig. 5 | Maps of canopy nitrogen. Canopy nitrogen concentration ($N_{mass'}$ %) estimated from spectra using PLSR for the (a) fifth growing season and (b) sixth growing season. Location of stands indicated with black boxes.



Extended Data Fig. 6 | Canopy nitrogen and stem biomass. Field-measured canopy nitrogen concentration was positively associated with spectrally predicted canopy nitrogen concentration in both (**a**) the fifth growing season and (**d**) the sixth growing season. Field-measured stem biomass was positively associated with both (**b**) field-measured canopy nitrogen concentration and (**c**) spectrally predicted canopy nitrogen concentration in the fifth growing season, and with both (**e**) field-measured canopy nitrogen concentration and (**f**) spectrally predicted canopy nitrogen concentration in the sixth growing season. Thick line represents the regression line (*P* < 0.001).



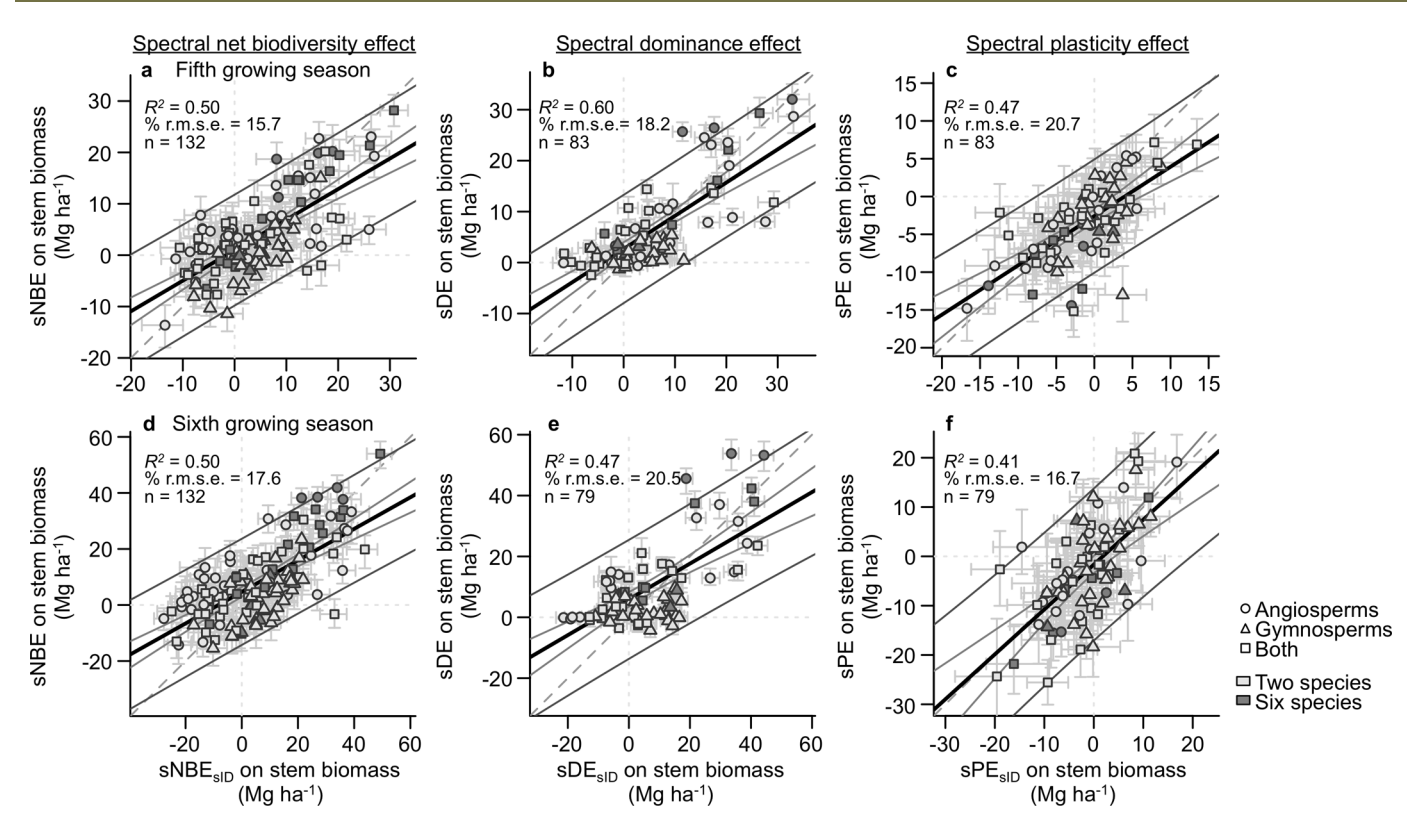
Extended Data Fig. 7 | Wavelengths of importance within PLS-DA models. Wavelengths of importance in distinguishing species within partial least squares discriminant analysis (PLS-DA) models (red) shown alongside the PLSR model of stem biomass (grey, unchanged in all panels). The variable importance index represents the reduction of sums of squares⁴⁹. Solid lines indicate the mean and shading indicates the 95% confidence intervals around the mean importance value for each wavelength across the 1000 model iterations. Vertical lines highlight the 20 most important wavelengths on average across the model iterations. Noisy and water absorption wavelengths are omitted.



Extended Data Fig. 8 | Spectral assignments of the species composition of stands. Species assignments based on PLS-DA. Two-species compositions were not present on all four blocks (indicated by asterisks): Pg-Qru was planted in place of Pg-Qro on Block B, and Pg-As was planted on two stands in Block D with one stand in place of Pa-As.

	Reference											
Predicted	Acer platanoides	Acer saccharum	Betula papyrifera	Betula pendula	Quercus robur	Quercus rubra	Larix decidua	Larix Iaricina	Picea abies	Picea glauca	Pinus strobus	Pinus sylvestris
Acer platanoides	0.863	0.039	0.014	0.000	0.054	0.033	0.004	0.007	0.006	0.001	0.003	0.002
Acer saccharum	0.008	0.928	0.000	0.000	0.000	0.003	0.002	0.005	0.001	0.015	0.000	0.000
Betula papyrifera	0.003	0.000	0.984	0.000	0.004	0.031	0.014	0.012	0.014	0.000	0.000	0.000
Betula pendula	0.009	0.000	0.000	1.000	0.001	0.017	0.017	0.043	0.005	0.005	0.000	0.002
Quercus robur	0.077	0.001	0.000	0.000	0.826	0.045	0.036	0.007	0.000	0.011	0.003	0.005
Quercus rubra	0.018	0.003	0.000	0.000	0.060	0.848	0.002	0.003	0.025	0.015	0.002	0.003
Larix decidua	0.002	0.006	0.001	0.000	0.015	0.003	0.744	0.185	0.014	0.003	0.008	0.002
Larix Iaricina	0.010	0.004	0.000	0.000	0.010	0.014	0.077	0.638	0.000	0.017	0.012	0.001
Picea abies	0.000	0.007	0.000	0.000	0.000	0.002	0.045	0.002	0.891	0.026	0.015	0.006
Picea glauca	0.000	0.012	0.001	0.000	0.004	0.000	0.038	0.044	0.029	0.896	0.006	0.015
Pinus strobus	0.001	0.000	0.000	0.000	0.024	0.004	0.021	0.048	0.000	0.005	0.946	0.002
Pinus sylvestris	0.009	0.000	0.000	0.000	0.000	0.000	0.000	0.006	0.013	0.007	0.005	0.962

Extended Data Fig. 9 | Confusion matrix for PLS-DA species assignments in monoculture. The reference species identity of pixels (columns) and the predicted species identity of pixels (rows) from PLS-DA calibrated with pixels drawn from monoculture stands in their fifth and sixth growing seasons. Values are the mean proportion of pixels assigned to a given species using the validation data subset in each iteration. Presented in coarse phylogenetic order, separating angiosperms from gymnosperms.



Extended Data Fig. 10 | Spectrally determined diversity effects on stem biomass calculated with remotely sensed species composition. Models whereby spectra were first used to predict the species composition of stands before calculating the net biodiversity effect (sNE_{siD}) (\mathbf{a} , \mathbf{d}), spectral dominance effect (sDE_{siD}) (\mathbf{b} , \mathbf{e}) and spectral plasticity effect (sPE_{siD}) (\mathbf{c} , \mathbf{f}) on stem biomass were each associated with their counterparts that were spectrally predicted using the known species composition of stands (sNBE, sDE and sPE, respectively). The top row (\mathbf{a} - \mathbf{c}) shows the fifth growing season and the bottom row (\mathbf{d} - \mathbf{f}) shows the sixth growing season. Error bars show 95% confidence intervals among the 1000 model iterations. Thick line represents the regression line (P<0.001), dark grey lines represent the 95% prediction interval, and light grey lines represent the 95% confidence interval of the models. Dashed grey line shows 1:1. Sample sizes differ among panels; all panels are limited to the subset of stands that were not monocultures or spectrally identified as such, and sDE and sPE are also limited to those stands where leaf area was measured.

nature research

Corresponding author(s):	Laura Williams		
Last updated by author(s):	Aug 27, 2020		

Reporting Summary

Nature Research wishes to improve the reproducibility of the work that we publish. This form provides structure for consistency and transparency in reporting. For further information on Nature Research policies, see our Editorial Policies and the Editorial Policy Checklist.

For all statistical analyses, confirm that the following items are present in the figure legend, table legend, main text, or Methods section,

_				
5	ta:	tı۹	ว†เ	2

n/a	Confirmed
	$oxed{\boxtimes}$ The exact sample size (n) for each experimental group/condition, given as a discrete number and unit of measurement
	🔀 A statement on whether measurements were taken from distinct samples or whether the same sample was measured repeatedly
	The statistical test(s) used AND whether they are one- or two-sided Only common tests should be described solely by name; describe more complex techniques in the Methods section.
\boxtimes	A description of all covariates tested
	🔀 A description of any assumptions or corrections, such as tests of normality and adjustment for multiple comparisons
	A full description of the statistical parameters including central tendency (e.g. means) or other basic estimates (e.g. regression coefficient) AND variation (e.g. standard deviation) or associated estimates of uncertainty (e.g. confidence intervals)
	For null hypothesis testing, the test statistic (e.g. <i>F</i> , <i>t</i> , <i>r</i>) with confidence intervals, effect sizes, degrees of freedom and <i>P</i> value noted <i>Give P values as exact values whenever suitable.</i>
\boxtimes	For Bayesian analysis, information on the choice of priors and Markov chain Monte Carlo settings
\boxtimes	For hierarchical and complex designs, identification of the appropriate level for tests and full reporting of outcomes
	\boxtimes Estimates of effect sizes (e.g. Cohen's d , Pearson's r), indicating how they were calculated
	Our web collection on statistics for biologists contains articles on many of the points above.

Software and code

Policy information about availability of computer code

Data collection

The Fieldspec Pro RS3 software (Analytical Spectral Devices, Boulder, CO, USA) was used to collect leaf spectra. Atmospheric correction for AVIRIS-NG was made using ATREM (Gao, B.C., K. H. Heidebrecht, and A. F. H. Goetz, Derivation of scaled surface reflectances from AVIRIS data, Remote Sens. Env., 44, 165-178, 1993).

Data analysis

ENVI (5.2) was used to resample pixels (Harris Geospatial Solutions, Inc., Broomfield, CO, USA), and Python 2.7 was used to map canopy nitrogen. Data analyses were completed in R (v3.5.1) with R packages pls (v2.7-0) and caret (v6.0-81). Model coefficients and example code for the new PLSR and PLS-DA models developed within the paper are available on the Data Repository for University of Minnesota: http://hdl.handle.net/11299/215251.

For manuscripts utilizing custom algorithms or software that are central to the research but not yet described in published literature, software must be made available to editors and reviewers. We strongly encourage code deposition in a community repository (e.g. GitHub). See the Nature Research guidelines for submitting code & software for further information.

Data

Policy information about <u>availability of data</u>

All manuscripts must include a data availability statement. This statement should provide the following information, where applicable:

- Accession codes, unique identifiers, or web links for publicly available datasets
- A list of figures that have associated raw data
- A description of any restrictions on data availability

AVIRIS-NG data can be downloaded from https://aviris-ng.jpl.nasa.gov/alt_locator/. Image level spectra, canopy nitrogen predictions, and associated plot measurements (including stem biomass, species proportions, field-based canopy nitrogen) are publicly available on the Data Repository for University of Minnesota: http://hdl.handle.net/11299/215251.

Field-specifi	c reporting
Please select the one below	w that is the best fit for your research. If you are not sure, read the appropriate sections before making your selection.
Life sciences	Behavioural & social sciences
For a reference copy of the docum	nent with all sections, see nature.com/documents/nr-reporting-summary-flat.pdf
Ecological, e	volutionary & environmental sciences study design
	n these points even when the disclosure is negative.
Study description	Here we examined whether imaging spectroscopy data can detect diversity effects on biomass across a tree diversity experiment. The tree diversity experiment is composed of 192 plots representing 48 different combinations of 12 common, temperate-boreal tree species and replicated on four experimental blocks. Assemblages were chosen to represent a gradient in species richness and functional diversity (each species in monoculture, 30 two species mixtures and 12 six species mixtures). Each plot was 2.8 m by 2.8 m containing 49 trees planted in a grid with 0.4 m spacing. Data were collected over two years when the plots were in the fifth and sixth growing season and canopies were largely closed.
Research sample	The research sample consists of two AVIRIS-NG images (each with 432 bands of 5 nm spectral resolution ranging from 380-2510 nm and spatial resolution of 0.8 m) along with field-based measurements collected across the tree diversity experiment composed of 192 plots.
Sampling strategy	Data were collected across all 192 plots within the tree diversity experiment with the exception of the line-intercept measurements of leaf area and leaf level spectra. All trees within the experiment were censused for diameter and height. Line-intercept measurements were collected on a subset of 128 plots in 2014 and 123 plots in 2015 (plots were omitted due to the time required to collect these data; the sampled subset of 41 to 46 of 48 assemblages on three of the four experimental blocks was chosen to represent the gradient in diversity whilst retaining replication across blocks, and were chosen prior to data analysis). Line intercept measurements were collected for 15 lines per plot; this number was chosen from previous sampling efforts. For leaf level spectral reflectance (used to map canopy nitrogen), one or two leaves or samples of conifer needles (mature and fully expanded) were collected from each of the top, middle and bottom of the crown of three trees per species on a subset of plots (36 plots within one block in 2014 and 39 plots within two blocks in 2015), and spectra were measured on three areas per leaf with five measurements per area.
Data collection	AVIRIS-NG images were acquired and processed by NASA Jet Propulsion Laboratory. Measurements of leaf-level spectral reflectance to map canopy nitrogen were led by John Couture with assistance from Anna Schweiger, Aidan Mazur and Melanie Sinnen, using an ASD FieldSpec 3 spectroradiometer (Analytical Spectral Devices, Boulder, CO, USA). Censuses of the diameter (with calipers) and height (with measuring pole) of all trees were led by Artur Stefanski with assistance from Karen Rice, Raimundo Bermudez and interns. Line intercept measurements of leaf area (with custom designed rig) were collected by Laura Williams with assistance from interns.
Timing and spatial scale	AVIRIS-NG images were acquired on August 25, 2014 and August 30, 2015. Leaf-level spectral reflectance was measured over one week in August of 2014 and one week in August of 2015. Trees were censused for diameter and height annually at the end of each growing season (September-October). Line intercept measurements of leaf area were taken over approximately one month in August of 2014 and 2015 when plots were at peak leaf area. All measurements were taken within the tree diversity experiment, which occupies an area of approximately 0.4 ha and is composed of 192 stands that each measure 2.8 m by 2.8 m.
Data exclusions	Noisy and water absorption bands were excluded from spectra prior to analysis. Line intercept measurements were collected on a subset of plots each year, as described above, with subsequent calculations and analyses (e.g., the spectral dominance and plasticity effects) completed using this subset of plots.
Reproducibility	All data were collected twice (once in 2014 and again in 2015). Two sets of spectral models were calibrated one using data from both years combined and another for each year separately and both the fit of these models and results from subsequent calculations of diversity effects were found to be comparable.
Randomization	In establishing the tree diversity experiment, two and six species mixtures were chosen to represent a gradient in functional diversity while maintaining approximately even representation of each species. Species were arranged within plots at random with rules to avoid clumping, and mixtures were arranged at random within experimental blocks. The 15 line intercept measurements per plot were located at random. Individual trees sampled for leaf-level spectral reflectance (per species and stand) were selected at random.
Blinding	Imaging spectroscopy data and field data were collected by separate teams. Data collectors could not be blinded to the species composition of plots when collecting field-based data.

Field work, collection and transport

Did the study involve field work?

Field conditions

The study site has a mean annual air temperature of 4.8 °C, an annual precipitation of 783 mm, and a short growing season of approximately 4 to 5 months. The site is flat, has a sandy loam soil, and was formerly forested.

-
-
α.
=
~
_
-
alule
r Leseal
_
4
I L
\mathcal{C}
Ā
Վե
σ
gi
\subseteq
_
$\overline{\alpha}$
α
7
E POI LI
Ξ
Leborning st
rs fundament
Leborning sur
reporting sum
reporting sum
reporting surin
reporting summ
reporting summa
reporting summa
reporting summar
reporting summary

ì	
٠	2
	≟
	$\stackrel{\checkmark}{\sim}$
3	
	$\bar{\sim}$
	\sim

Location	The study was conducted on a tree diversity experiment planted at the University of Minnesota's Cloquet Forestry Center (Minnesota, USA, 46° 40′ 46″ N, 92° 31′ 12″ W , 382 m.a.s.l.)
Access & import/export	Data were collected in compliance with local, national and international laws.
Disturbance	Minimal numbers of leaves were harvested as needed for measurements.

Reporting for specific materials, systems and methods

We require information from authors about some types of materials, experimental systems and methods used in many studies. Here, indicate whether each material, system or method listed is relevant to your study. If you are not sure if a list item applies to your research, read the appropriate section before selecting a response.

Materials & experimental systems		Methods		
dy	n/a	Involved in the study		
	\boxtimes	ChIP-seq		
nes	\boxtimes	Flow cytometry		
nd archaeology	\bowtie	MRI-based neuroimaging		
er organisms		•		
participants				
h of concern				
	mental systems dy nes nd archaeology er organisms participants h of concern	n/a nes and archaeology er organisms participants		